Île Dumet (Armorican Massif, France) and its glaucophane eclogites: the little sister of Île de Groix

Gaston Godard, David C. Smith, Damien Jaujard, Sidali Doukkari

Eur. J. Mineral., 36, 99–122, 2024
https://doi.org/10.5194/ejm-36-99-2024

European Journal of Mineralogy
Open Access

Île Dumet (Armorican Massif, France) and its glaucophane eclogites: the little sister of Île de Groix

Gaston Godard[1], David C. Smith[2,☆], Damien Jaujard[3], and Sidali Doukkari[4,5]

[1]Institut de Physique du Globe de Paris, Université Paris Cité,
1 rue Jussieu, 75238 Paris CEDEX 05, France
[2]1312 Chemin de la Sonnière, 38850 Villages du Lac de Paladru, France
[3]INSPE Créteil, Université Paris-Est Créteil, 1 rue Jean Macé, 94380 Bonneuil-sur-Marne, France
[4]Laboratoire de Géodynamique, Géologie de l'Ingénieur et de Planétologie, FSTGAT–USTHB, B.P. 32,
El Alia, Dar el Beïda, 16111 Algiers, Algeria
[5]Département SNV, Faculté des Sciences, Université d'Alger 1, 2 rue Didouche Mourad, Algiers, Algeria
[☆]retired

Correspondence: Gaston Godard (godard@ipgp.fr)

Received: 31 July 2023 – Revised: 23 November 2023 – Accepted: 25 November 2023 – Published: 19 January 2024

Abstract. Blueschist-facies rocks are scarce within the Variscan orogen. Two main occurrences are known in the Armorican Massif (NW France), at Île de Groix and Bois-de-Céné. Another glaucophane occurrence was discovered in 1988 but went unnoticed; it is located on Île Dumet, an uninhabited island off the coast of southern Brittany, in the estuary of the river Vilaine. Orthogneiss occurs on the SW half of the island; the original granitoid magma had intruded mica schists on the NE half, where numerous 1 to 10 m long boudins of mafic rocks occur. These lenses are typically retrogressed into plagioclase-bearing amphibolite, but a few contain remnants of glaucophane-bearing eclogite, which also occurs as numerous loose blocks along the NE coast of the island, suggesting that the best-preserved eclogites lie in situ offshore in that direction.

The glaucophane eclogites contain garnet, omphacite, quartz, amphibole, clinozoisite/epidote, minor phengite, paragonite, rutile and rare apatite. Prograde metamorphic evolution is indicated by garnet crystals zoned from Mn-rich cores to Mg-richer rims (typically (core →rim): $Alm_{44\rightarrow58}$ $Prp_{1\rightarrow12}$ $Grs_{33\rightarrow29}$ $Sps_{22\rightarrow1}$) and amphibole grains with glaucophane nuclei and Ca–Na-amphibole overgrowths that show sharp transitions, supporting evolution through a solvus, as predicted by the thermodynamic modelling. Modelling of the P–T conditions using the P–T pseudosection technique indicates a peak of metamorphism at about 620 °C and 16 kbar. The retrograde evolution of the metabasites is evidenced by the late formation of albite, titanite and ferro-actinolite. The surrounding mica schists, composed of quartz, garnet, phengite, paragonite and chlorite, were also largely retrogressed during exhumation. The orthogneiss of the SW part of the island does not show clear evidence of high-pressure metamorphism, since the magmatic feldspars are still preserved, similarly to the orthogneiss of Les Sables Rouges on the island of Groix.

Île Dumet and the western part of the Vilaine estuary represent a blueschist-facies equivalent to Île de Groix (Brittany) and Bois-de-Céné (Vendée) on the mainland. All three occurrences occupy the centres of wide synforms whose concentric units are, from rims to core (i.e. from base to top), (a) a high-T migmatitic basement; (b) Cambro-Ordovician metasediments and acid metavolcanites ("porphyroids"); and (c) blueschist-facies mica schists and metabasites, serpentinites, and minor orthogneisses derived from a pre-Variscan oceanic accretionary prism. There are about 10 similar occurrences within the Ibero-Armorican Arc, forming a discontinuous high-pressure belt, but most of them have remained unnoticed due to a high degree of retrogression.

Published by Copernicus Publications on behalf of the European mineralogical societies DMG, SEM, SIMP & SFMC.

1 Introduction

At the western edge of the European Variscides, the South Armorican Domain (Armorican Massif, NW France; Fig. 1a, b) is part of the Ibero-Armorican Arc, which has been interpreted as the result of a collision between the Laurussia and Gondwana continents during the Variscan orogeny (see reviews in Ballèvre et al., 2014; Díez Fernández et al., 2016; Martínez Catalán et al., 2020). In this context, blueschist-facies rocks most likely belong to a palaeo-subduction zone, highlighting the suture zone. However, glaucophane-bearing rocks are rare in the South Armorican Domain, where only two occurrences are known to date, at Île de Groix – a famous site that has been extensively studied since 1883 – and at Bois-de-Céné on the mainland (Fig. 1b). Another glaucophane occurrence was reported in 1988 on the 0.09 km^2 uninhabited island of Île Dumet. This small island is located off the coast of southern Brittany, about 65 km SE of Île de Groix and 60 km NW of Bois-de-Céné, almost at equal distance between these two occurrences (Fig. 1b, c). However, the Dumet finding went unnoticed because it was not taken into account in the geodynamic models of the Ibero-Armorican Arc and was not even mentioned in the latest edition of the 1 : 1 000 000 geological map of France.

After a brief description of the general geology of Dumet Island, we propose a detailed mineralogical and petrological study of the rocks observed there, in particular the lenses of glaucophane-bearing eclogite and their surrounding phengite- and paragonite-bearing mica schists, whose metamorphic evolution is determined by modelling P–T pseudosections. Finally, we discuss the geological and geodynamical implications of this new occurrence, showing that similar occurrences of glaucophane-bearing rocks are more numerous in the Ibero-Armorican Arc than previously thought.

2 Geological presentation of Dumet Island

Île Dumet is an uninhabited island of 8.5 ha located on the SW coast of the Armorican Massif, in western France (lat 47.412°, long −2.620°), off the estuary of the Vilaine River and about 6 km from the picturesque village of Piriac-sur-Mer (hereafter Piriac) on the mainland. Throughout history, the island has been intermittently inhabited since the Neolithic period (Levillayer and Moreau, 2019; Levillayer, 2020) and has also been occupied by the Saxons, Vikings, Spanish and English, as well as a few hermits. This turbulent history has fuelled several legends, including the existence of alleged treasure buried on the island (e.g. Delorme, 2020). In 1913, Alphonse Berget calculated that Dumet Island was the pole of the "continental hemisphere" that includes most of the Earth's landmass (Berget, 1913; e.g. Affholder, 2002), and he therefore recommended the Dumet meridian as the reference for universal time, but, as we now know, the Greenwich meridian was preferred. In 1990, Dumet Island became an ornithological reserve of the French Conservatoire du Littoral (Pierronnet, 1997), and its access is strictly regulated and in fact quite difficult.

2.1 Previous geological studies

The only buried treasure of Dumet Island is none other than its rocks, which have aroused the interest of ancient and modern geologists. Édouard Richer (1820–1823, vol. 2, p. 17) was the first to describe the island from a geological point of view. He observed gneisses, mica schists and especially some "*grünstein*" (green rock) with chlorite and "diallage" (i.e. clinopyroxene). However, only "gneiss" and "micaschist" appear on the first geological maps published in the 19th century. Later, Pic (1936) mentioned pebbles "in which one can find garnet, epidote, pyroxene, amphibole".

It was in fact Claude Audren who carried out the first detailed geological study of Dumet Island, as part of a wider survey of the Vilaine estuary (Audren, 1974, 1987). In particular, he drew up a geological map of the island, distinguishing between an orthogneiss in the south and mica schists with amphibolite pods in the north. He sent five orthogneiss samples to Jean-Jacques Peucat for dating by the Rb–Sr method (419 ± 12 Ma: Peucat, 1983).

In the 1980s, Bernard Lasnier discovered glaucophane eclogite relics in the amphibolite pods. He published his findings in a monograph on the geology of Dumet Island (Baudouin et al., 1988), which remains the most complete source of information on the geology of the island but has been largely ignored because it was published in a regional periodical. Some electron-microprobe spot analyses of clinoamphiboles, including glaucophane, were carried out by Lasnier and Smith (1989) and Smith et al. (1999), who noted the analogy between Dumet and Groix islands. The evidence for a high-pressure (HP) metamorphism at Dumet Island was echoed in the leaflet of the geological map at 1/50 000 (Augier et al., 2010).

2.2 Geological overview

Although largely covered by Quaternary sediments (Dresch, 1964), the bedrock of Dumet Island is very well exposed on the foreshore, which is largely uncovered at low tide (Fig. 2). The island is geologically divided into two main parts (Figs. 1c, 2):

a. In the north, mica schists, alternating with some more quartzitic levels, contain many 1 to 10 m long lenses of metabasite mainly composed of amphibole, plagioclase and garnet, which are derived from rarely preserved glaucophane eclogite (Fig. 3a). The best-preserved eclogites are actually visible on the beach south-east of Fort de Ré (Figs. 1c, 2), in the form of many loose ovoid blocks that can reach 0.4 m in length, suggesting that the best glaucophane–eclogite in situ occurrences are at sea towards the north-east.

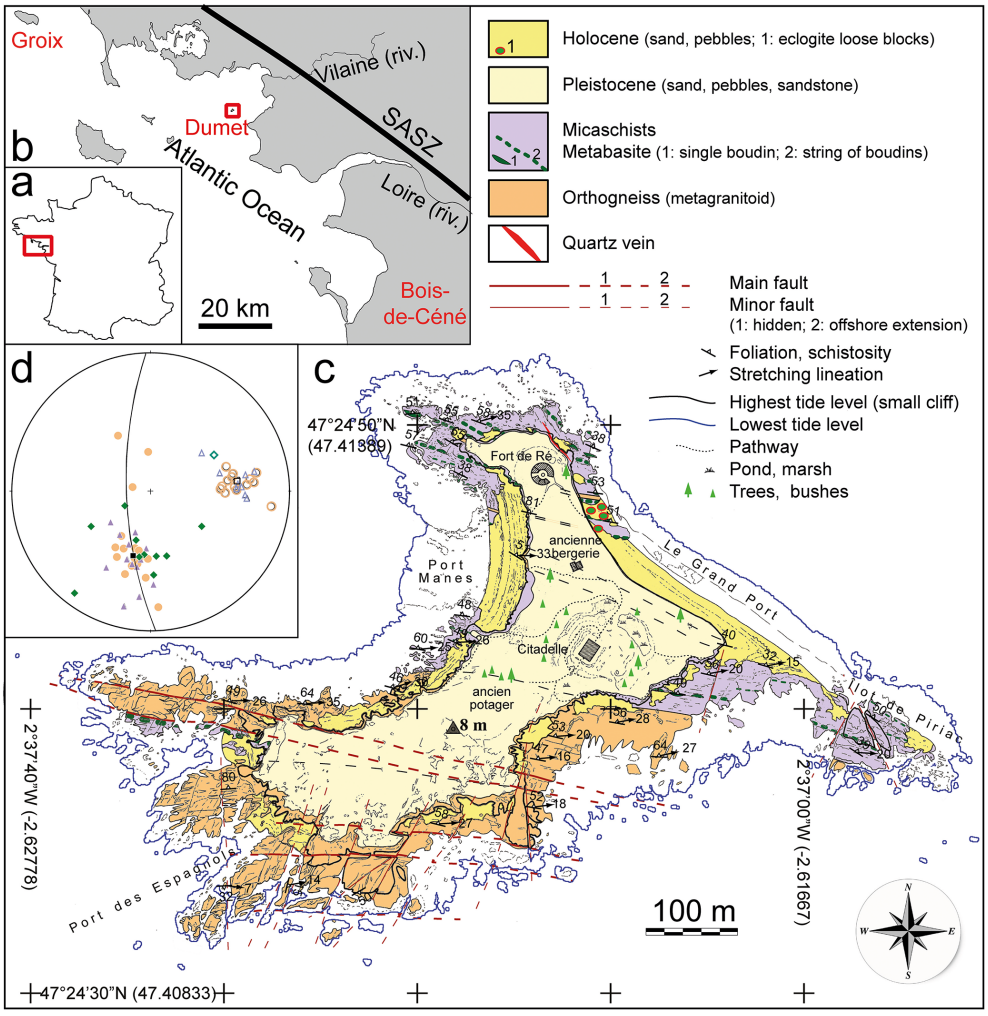

Figure 1. Structure and geological map of Île Dumet. **(a)** The Atlantic location of Dumet Island. **(b)** Dumet Island on the west coast of Armorica, south-east of Île de Groix (SASZ: South Armorican Shear Zone). **(c)** Geological map of Dumet Island. The thick black and blue lines represent the coastline at the highest and lowest tide levels, respectively; the foreshore as represented on the map corresponds to an ordinary low tide; the topographic background is modified after Yves Bodeur (in Baudouin et al., 1988). **(d)** Structural data of Île Dumet (partly from Audren, 1987). Equal-angle projection in the lower hemisphere. Filled symbols: poles of main foliation (orthogneiss, metabasites) and schistosity (mica schists). Open symbols: stretching lineation. Brown circles: orthogneiss; purple triangles: mica schists; green diamonds: metabasites; black squares: mean vectors; curve: cylindrical best fit of poles to main foliation/schistosity.

b. The southern part of the island consists mainly of acidic orthogneiss. It encloses on the west coast a large stretched enclave of mica schists with metabasite lenses (Fig. 1c), similar to what occurs on the northern part of the island; everywhere, the immediate host rock of the metabasite pods is mica schist, never orthogneiss. This orthogneiss also locally shows narrow apophyses and veins intensely stretched within the mica schists, parallel to the main foliation (Figs. 1c, 3b); the largest of these veins, about 10 metres thick, crosses the island below the former sheep barn (*bergerie*) with a strike of 114° (Figs. 1c, 2), whilst other metre-thick veins are visible here and there in the mica schists (e.g. Fig. 3b). These observations suggest that the magmatic protolith has intruded the mica schists before being intensely deformed. Within a zone a few metres thick near the contact with the mica schists, this orthogneiss appears to be more leucocratic, being enriched in white mica.

The EW-oriented S-dipping foliation in the orthogneiss is essentially parallel to the main schistosity in the mica schists, and so are the less pronounced E-dipping stretching lineations (Fig. 1d). At the island scale, these foliation and schistosity planes, termed S_2 by Audren (1987), are slightly dispersed around an axis parallel to the stretching lineation L_2 (the best cylindrical fit of the S_2 poles is approximately perpendicular to L_2; Fig. 1d). Audren (1987) observed early structures in mica schists, in particular an early schistosity

(S_1) isoclinally folded parallel to the main schistosity S_2. The metabasite boudins form discontinuous alignments (Fig. 1c), which most likely result from the stretching of initially more or less continuous levels of a mafic protolith. The foliation and stretching lineation within these metabasite lenses are subparallel to those in their host rock but more irregular and scattered (Fig. 1d), presumably due to some disruption during boudinage.

3 Samples and methods

We were authorised to access the island for 2 consecutive days, which allowed us to complete a new geological map (Fig. 1c), make some quick structural observations (Fig. 1d) and collect 41 samples. We were also fortunate enough to observe 35 thin sections of rocks collected on the island in the 1980s by Bernard Lasnier. The study was completed on the mainland by the search, observation and petrological study of similar rocks, mostly mica schists and retrogressed metabasites, from the banks of the Vilaine estuary.

A selection of 34 samples, either from the island or from the mainland, were examined under a scanning electron microscope (SEM) and with an electron microprobe (EMP). They were studied under a Zeiss Supra 55 VP SEM at Paris-Sorbonne Université, in particular to produce backscattered-electron (BSE) images and X-ray elemental maps. Image processing was carried out using Photoshop® (brightness and contrast adjustments; smoothing and enhancement filtering) and ENVI® (principal-component analysis, mineral classification). EMP analyses of the minerals were carried out using the Cameca SXFive electron microprobe at the Camparis laboratory in Paris (http://www.service-camparis.fr/, last access: 10 January 2024). The analytical conditions were a beam current of 10 nA, an acceleration voltage of 15 kV and a spot diameter of about 1 µm. Natural minerals and synthetic oxides were used as standards. The structural formulae are calculated on the basis of quantities of O and OH anions depending on the mineral group, i.e. for garnets, O_{12} and $Fe^{3+} = 2 - Al_{total} - Cr - 2 \times Ti$, with Al^{IV} set at zero; for epidotes, $O_{12}(F,OH)_1$ and $Fe^{3+} = Fe_{total}$; for micas, $O_{20}(OH,F)_4$, $Fe^{3+} = 0$; for chlorites, $O_{20}(OH)_{16}$, $Fe^{3+} = 0$; for feldspars, O_8, $Fe^{3+} = Fe_{total}$; for pyroxenes, O_6, Fe^{3+} value corresponds to a total of four cations; for amphiboles, the procedure of Hawthorne et al. (2012) and Locock (2014) was used, giving a range of Fe^{3+} values for which the cation distribution in the T, C, B and A sites is correct; since the amount of ferric iron is limited in mafic rocks, we finally chose the minimum value of Fe^{3+}, which is generally zero.

In order to reconstruct the metamorphic evolution of the rocks, we have studied in greater detail four samples representative of the rocks observed on the island, namely an eclogite (ID25a), a garnet glaucophanite (ID25b), a mica schist (ID13) and an orthogneiss (ID17):

a. The first two samples (ID25a and ID25b) come from one of the 40 cm sized loose blocks of *glaucophane eclogite* found on the beach, east of Fort de Ré. This block was chosen over the strongly retrogressed eclogites and amphibolites outcropping nearby because of its well-preserved HP mineralogy. It shows an alternation of bands, analysed and modelled separately, of (i) eclogite (omphacite + garnet + epidote + quartz; ID25a: Fig. 4a) and (ii) garnet glaucophanite (glaucophane + garnet + minor quartz; ID25b: Fig. 4b). Its study was complemented by that of other metabasites, either well-preserved glaucophane eclogites (ID1, ID9) or metabasites retrogressed to garnet amphibolites (ID16, ID33), sampled on the foreshore (ID1, ID9) or from the many mafic boudins on the north of the island (ID16: 47.4113, −2.6185; ID33: 47.4136, −2,6197).

b. The third sample (ID13) is a *mica schist*, containing garnet, chlorite, phengite, paragonite, albite and quartz, collected in situ (47.4113, −2.6183) at a short distance from the retrogressed eclogite lens in Fig. 3a.

d. Finally, a representative sample of the southern *orthogneiss* (ID17) was collected in situ (47.4111, −2.6189) close to the contact with the mica schists, at about 50 m from the previous sample ID13.

We calculated isochemical P–T pseudosections for three of these selected samples (ID25a, ID25b and ID13). The last sample (ID17), although studied in detail, was not retained as suitable for modelling a P–T pseudosection because it was not fully equilibrated during metamorphism, having preserved many minerals of the magmatic protolith, in particular feldspars. Since a P–T pseudosection is valid for a given bulk chemical composition, the three samples were crushed, ground and analysed by inductively coupled plasma–optical emission spectrometry (ICP-OES) for major elements and by ICP–mass spectrometry (ICP-MS) for trace elements, at the Service d'Analyse des Roches et des Minéraux in Nancy, France, according to protocols detailed at http://sarm.cnrs.fr (last access: 10 January 2024). The resulting bulk-rock compositions (Table 1) were slightly modified for modelling purposes. Total CaO was reduced based on the amount of P_2O_5 sequestering Ca in apatite, which is not taken into account in the modelling. The negligible amount of Cr_2O_3 was added to Al_2O_3, since Cr^{VI} substitutes for Al^{VI} in many minerals. H_2O was assumed to be in excess, which seems reasonable given the abundance of hydrous minerals and the loss-on-ignition value (LOI; Table 1). Since the cores of the garnet crystals are isolated after their growth, the effective chemical composition of the system differs slightly from the bulk-rock composition. However, due to the very small size of the garnet crystals – typically 0.4 mm in diameter (Fig. 4) – this fractionation phenomenon was not considered critical and was therefore neglected. Finally, the amount of O associated with Fe^{3+} was estimated from the structural formulae

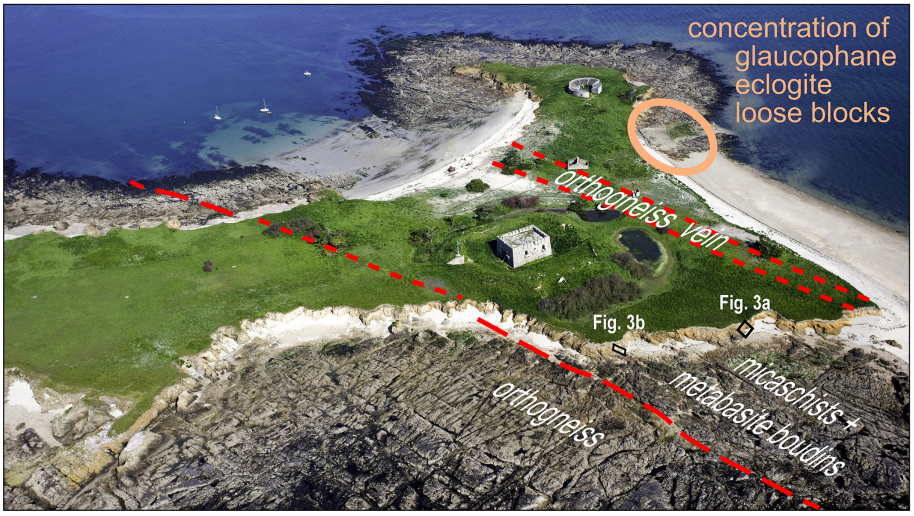

Figure 2. Aerial photograph of Île Dumet, looking NNW. Dashed red line: contact between orthogneiss and mica schists with metabasite lenses; orange ellipse: occurrence on the foreshore of numerous loose blocks of glaucophane eclogite, 0.1–0.4 m in size; © Valery Joncheray.

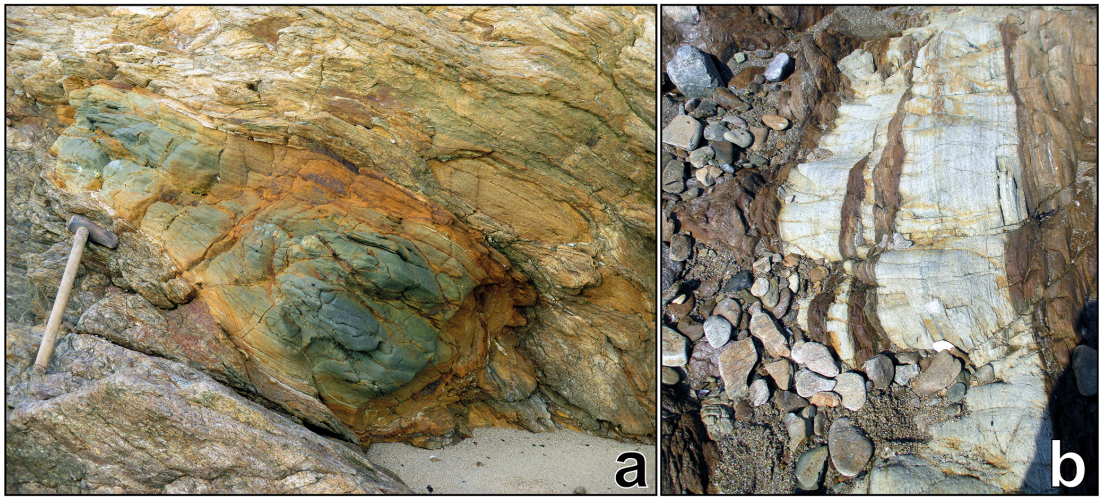

Figure 3. Field macrostructures. **(a)** A 1 m sized blue-green lens of retrogressed eclogite, boudinaged within mica schist and characteristically more retrogressed towards its margins (47.4116, −2.6184). **(b)** A 0.5 m wide vein of banded orthogneiss (light grey) within mica schists (dark grey-brown; 47.4112, −2.6189). The foliation in the orthogneiss is parallel to the main schistosity of the mica schists, indicating that the two rocks have been deformed together; the orthogneiss vein shows ramifications and enclaves suggesting that it is derived from an earlier granitoid that intruded the mica schist protolith.

and molar proportions of the minerals in the main paragenesis, bearing in mind of course that this value may have changed during metamorphic evolution. The molar proportion of the minerals in each rock was estimated by the least-squares method, using the chemical composition of the bulk rock and that of the minerals; the result (Table 1) was considered satisfactory if the residuals were small and the stoichiometric coefficients obtained for the minerals were positive (see Godard, 2009, for the method and software). These molar quantities were then converted into volume percentages (Table 1), using the molar volumes of Holland and Powell (2011).

The pseudosection modelling was carried out in the chemical system K_2O–Na_2O–CaO–FeO–MgO–Al_2O_3–SiO_2–MnO–H_2O–TiO_2–O, using the software THERMOCALC v3.45 (Powell and Holland, 1988) and an updated version of the thermodynamic data set of Holland and Powell (2011) (ds62 of February 2012). The activity–composition models used for solid solutions are as follows: Green et al. (2016) for omphacitic clinopyroxenes and the clinoamphiboles, "hornblende", actinolite, and glaucophane, which may be co-stable; White et al. (2014) for garnet, staurolite and chlorite; Smye et al. (2010) for phengite, muscovite and paragonite; Holland and Powell (2011) for epidote; and Hol-

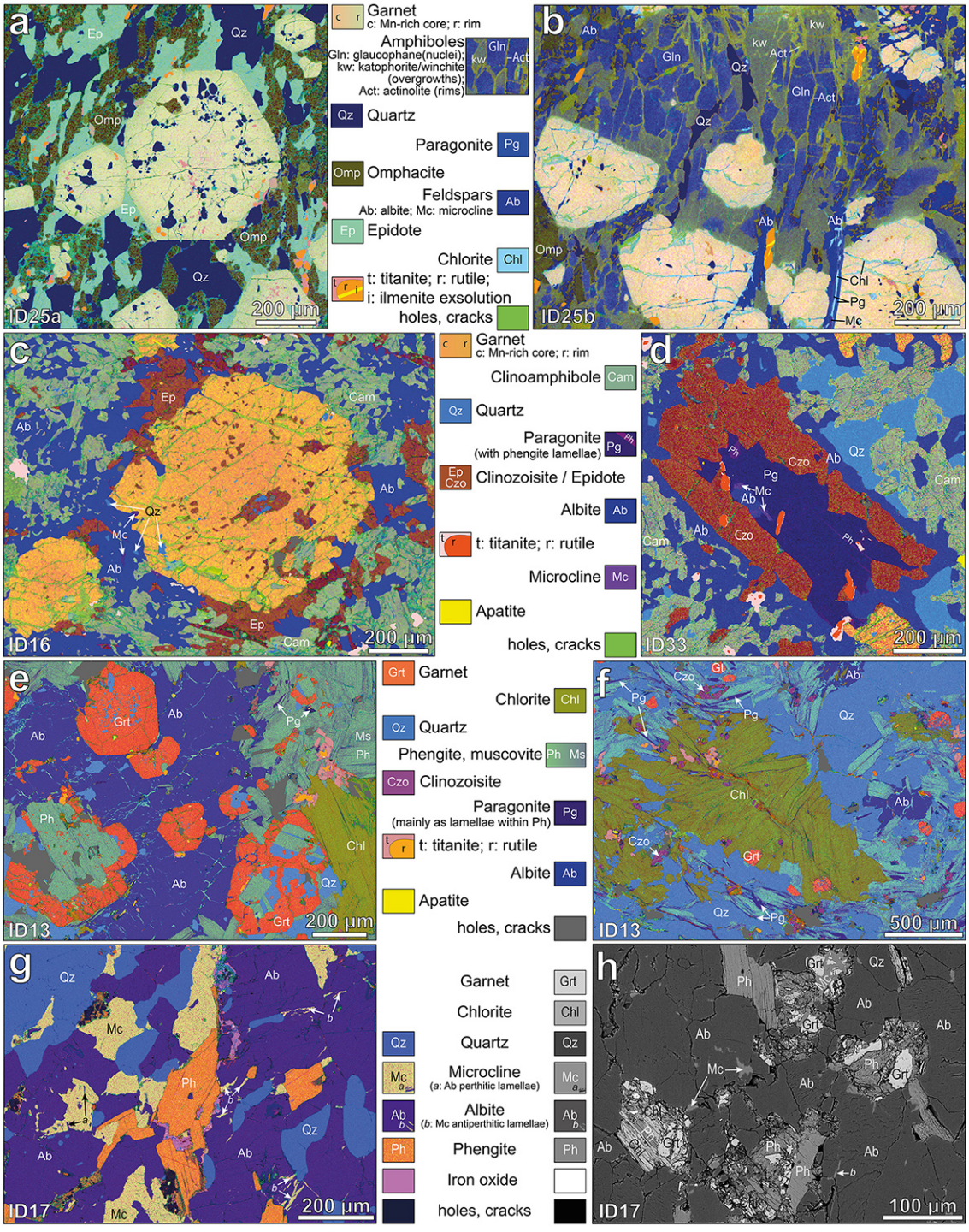

Figure 4. Rock microstructures. **(a–g)** Images elaborated by principal-component analysis of 11 element maps; **(h)** BSE image. **(a)** Eclogite band (sample ID25a). **(b)** Garnet glaucophanite band (sample ID25b); glaucophane crystals (Gln) show overgrowths of Na–Ca amphiboles (kw) in the foliation direction and are bordered by a thin film of late Ca amphibole, mainly actinolite (Act). **(c)** Retrogressed eclogite (sample ID16): garnet crystals are set in a matrix of clinozoisite, clinoamphibole and albite, with rare relics of quartz and rutile mainly transformed into titanite. **(d)** Retrogressed eclogite (sample ID33): a crystal of paragonite, with a few lamellae of exsolved phengite, is surrounded by a reaction corona of epidote and albite. **(e, f)** Mica schist (sample ID13): garnet crystals may show an atoll structure with a lagoon of phengite and quartz; the phengite flakes evolve towards muscovite at their edges and show exsolution lamellae of paragonite, which is absent from the matrix where albite is found instead; chlorite forms radiating aggregates possibly after another mineral; rutile is partially transformed into titanite. **(g, h)** Orthogneiss (sample ID17): exsolution lamellae of albite (*a*: perthite) and of microcline in albite (*b*: antiperthite) indicate a magmatic origin; Ca-rich garnet microcrystals associated with phengite and microcline are preferentially located at the contacts between chlorite (after biotite) and plagioclase.

Table 1. Compositions of the eclogite (ID25a), garnet glaucophanite (ID25b) and mica schist (ID13) used to model the P–T pseudosections. See Sect. 3 for details of the bulk-rock analyses and the calculation of the modal percentages; LOI: loss on ignition; Amp*: Ca–Na clinoamphibole.

Sample	Rock	Unit	SiO_2	Al_2O_3	Fe_2O_3	MnO	MgO	CaO	Na_2O	K_2O	TiO_2	P_2O_5	LOI	Total		
ID25a	eclogite	wt %	51.90	14.53	14.24	0.21	3.19	11.57	2.29	0.06	1.16	0.11	0.20	99.44		
ID25b	glaucophanite	wt %	48.68	14.51	17.65	0.23	5.80	7.77	3.52	0.07	1.38	< 0.10	−0.08	99.53		
ID13	mica schist	wt %	67.30	14.96	5.14	0.05	2.05	1.29	1.74	2.84	0.64	0.18	2.73	98.91		
Modal composition			Grt	Omp	Gln	Amp*	Qz	Ep	Chl	Ph	Pg	Ab	Rt	Ttn	Ap	
ID25a	eclogite	vol %	27.0	30.2		4.6	19.7	16.3		0.2	0.7		0.9		0.3	
ID25b	glaucophanite	vol %	31.7	20.2	21.5	16.6	6.2	0.0		0.3	2.4		1.0			
ID13	mica schist	vol %	2.4				41.3	0.0	9.2	31.3	0.0	13.7		1.2	0.7	
CIPW norm converted into vol.			Ap	Ilm	Mt	Ol	Opx	Cpx	Pl				Qz			
ID25a	eclogite	vol %	0.3	1.7	0.0		17.4	24.2	49.5	($Or_{0.7}$ $Ab_{41.0}$ $An_{58.3}$)			6.9			
ID25b	glaucophanite	vol %	0.0	1.7	0.0	15.5	30.1	11.4	41.3	($Or_{0.7}$ $Ab_{56.8}$ $An_{42.4}$)						
			As	Ba	Be	Bi	Cd	Ce	Co	Cr	Cs	Cu	Dy	Er	Eu	Ga	Gd
ID25a	eclogite	$\mu g\,g^{-1}$	0.69	7.6	0.47	0.15	0.29	7.51	27.8	7.0	0.08	10.6	3.45	2.24	0.965	23.1	2.84
ID25b	glaucophanite	$\mu g\,g^{-1}$	0.87	29.1	0.52	< 0.05	0.30	6.29	50.7	9.9	0.07	15.7	4.06	2.67	0.597	15.6	2.50
			Ge	Hf	Ho	In	La	Lu	Mo	Nb	Nd	Ni	Pb	Pr	Rb	Sc	Sb
ID25a	eclogite	$\mu g\,g^{-1}$	2.02	1.11	0.801	0.09	3.22	0.342	< 0.50	0.38	6.11	6.4	56.7	1.19	1.89	49.2	0.51
ID25b	glaucophanite	$\mu g\,g^{-1}$	1.55	1.38	0.936	0.06	2.49	0.434	1.00	0.48	5.18	12.2	3.02	0.98	2.38	58.1	0.49
			Sm	Sn	Sr	Ta	Tb	Th	Tm	U	V	W	Y	Yb	Zn	Zr	
ID25a	eclogite	$\mu g\,g^{-1}$	2.21	0.55	474.0	0.03	0.505	0.45	0.327	0.30	544	< 0.80	20.6	2.24	73.3	31.0	
ID25b	glaucophanite	$\mu g\,g^{-1}$	1.80	0.51	26.4	0.04	0.556	0.52	0.388	0.18	525	1.51	24.7	2.74	172	37.6	

land and Powell (2003) for plagioclase. Ordered low albite (Ab) was considered in addition to disordered plagioclase solid solution (Pl) because the peristerite miscibility gap can occur in low-T conditions. Low albite, lawsonite, rutile, titanite, quartz and water are considered pure phases.

Mineral abbreviations used hereafter are taken from Whitney and Evans (2010); "apfu" means "atoms per formula unit". Mineral compositions are often expressed as molar percentages of the end-members (e.g. $Or_{0.6}$ $Ab_{99.0}$ $An_{0.4}$ $Cls_{0.0}$). The margins of error given for the molar compositions and ratios are $\pm 1\sigma$. Latitude and longitude (negative westwards) are given in decimal degrees. A few figures (Figs. S1 and S2) and tables (Tables S1 and S2) are available in the Supplement.

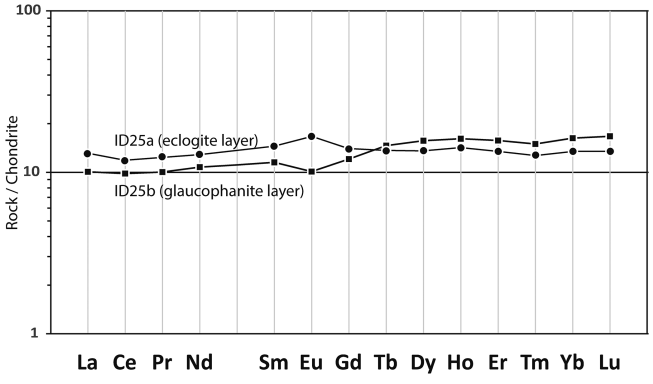

Figure 5. Rare-earth elements in glaucophane eclogite ID25. REE concentrations in the eclogite and garnet glaucophanite levels of sample ID25 are normalised to chondrite, using normalisation values from Evensen et al. (1978).

4 Petrological and mineralogical study

4.1 Metabasites

The best-preserved glaucophane eclogites of Île Dumet are provided by large blocks collected on the northern part of the island (e.g. samples ID1, ID9, ID25; Fig. 2). These huge loose blocks consist of a fine-grained banded rock, with alternating greenish and dark-blue bands, 1 to 10 cm thick, consisting of eclogite and garnet glaucophanite, respectively. Chemically, these levels differ mainly in their Ca and Na contents (Table 1) but show fairly similar chondrite-normalised rare-earth-element (REE) profiles (Fig. 5). Their crystals are oriented and define a foliation subparallel to the banding, which has therefore been transposed parallel to the foliation.

The eclogite bands (ID25a: Figs. 4a, S1a) are composed of the following: omphacite; subhedral garnet crystals whose diameters never reach 1 mm; abundant epidote ($X_{Fe^{3+}} = Fe^{3+}/(Fe^{3+} + Al + Mn^{3+} + Cr) = 0.215 \pm 0.028$); quartz; minor Ca–Na amphibole; and accessory rutile, fluorapatite and paragonite. The garnet crystals show a clear zonation, with cores richer in Ca and especially Mn and poorer in Mg than their rims (ID25a in Fig. 6a, d; core→rim: $Alm_{43.9\rightarrow57.8}$ $Prp_{0.9\rightarrow12.1}$ $Grs_{33.2\rightarrow29.3}$ $Sps_{22.0\rightarrow0.7}$; $X_{Mg} =$

$Mg/(Mg + Fe^{2+} + Mn) = 0.014 \rightarrow 0.172$). In these garnet crystals, numerous inclusions of quartz, epidote and titanite (in the core of the crystals) and rutile (at their edges) can be observed, as well as rare omphacite (Fig. 4a), which has a lower Na content (triangles in Fig. 7) than the omphacite in the matrix (ID25a: Na $= 0.414 \pm 0.029$ vs. 0.485 ± 0.017 apfu, respectively). The omphacite in the matrix is quite homogeneous (Fig. 7; e.g. ID25a: $Jd_{39.5 \pm 2.6}$ $Aeg_{9.1 \pm 2.4}$; $X_{Mg} = 0.809 \pm 0.028$); the slight apparent spread of its composition along a Jd_{+x} Aeg_{-x} vector (Fig. 7) is presumably related to the uncertainty in the stoichiometric estimation of Fe^{3+} (see Sect. 3). In some slightly retrogressed eclogite samples (e.g. ID9), a decrease in jadeite content occurs at the edges of the omphacite crystals, where jadeite is exsolved in the form of albite (see "towards Ab" in Fig. 7).

The garnet glaucophanite bands (ID25b: Figs. 4b, S1b) are composed mainly of clinoamphibole, subhedral garnet, omphacite and quartz, with minor rutile, paragonite, K-feldspar and late albite. The garnet crystals, generally smaller than those in the eclogite bands, are however similar in composition and zoning (ID25b in Fig. 6b vs. ID25a in Fig. 6a). They enclose minute inclusions of quartz, epidote, titanite, rutile, apatite and rare amphibole including glaucophane (ID9 in Table 2). Omphacite also has a composition quite similar to that of the neighbouring eclogite layers (ID25b vs. ID25a in Fig. 7; $Jd_{37.1 \pm 4.0}$ $Aeg_{13.6 \pm 3.7}$; $X_{Mg} = 0.856 \pm 0.030$). The amphibole crystals in the matrix, typically 0.2 mm in size, generally consist of a homogeneous nucleus of glaucophane (Gln in Fig. 4b; circles in Fig. 8c, d; Table 2), on which have grown, parallel to the foliation, overgrowths of a slightly zoned Ca–Na amphibole, katophorite or winchite (kw in Fig. 4b; Fig. 8a, b; squares in Fig. 8c, d; Table 2). Each crystal, thus elongated parallel to the foliation, is also bordered by a zone a few micrometres thick whose composition is Ca-rich and varies from pargasite/magnesio-hornblende to actinolite (Act in Fig. 4b; "+" in Fig. 8c, d). Actinolite also occurs along late fractures that cut the foliation. This general evolution from Na to Ca species is accompanied by a decrease in X_{Mg} to reach Fe^{2+}-rich ferrous species. Amphibole is also present around garnet, forming microcoronas of (ferro-)katophorite or (ferro-)pargasite ("×" in Fig. 8c, d; Table 2). Some large crystals of (ferro-)pargasite included in garnet seem to belong to the same generation of Fe-rich amphibole as that in the microcoronas (ID1 in Table 2; triangles in Fig. 8c, d); like the latter, they would have developed late at the expense of the host garnet rather than being trapped during its growth.

The generally fine-grained metabasites of the numerous lenses stretched within the mica schists (Fig. 3a) are essentially composed of subhedral crystals of garnet, commonly < 1 mm in size, and amphibole forming coarse symplectites with albite; clinozoisite (or epidote); and, incidentally, quartz, paragonite, apatite and titanite with internal relics of rutile (Figs. 4c, d, S1c, d; e.g. samples ID16 and ID33). The composition and zonation of the garnet crystals are very similar to those of the well-preserved eclogites, in particular with a core rich in Mn (Fig. 6c vs. 6a; Fig. 6d); they also contain inclusions of epidote, quartz, amphibole and titanite. Ca-rich clinoamphibole, most commonly pargasite, magnesio-hornblende or actinolite (Fig. 8c), forms symplectites with albite (ca. Ab_{98}). As in some glaucophane eclogites (see above), amphibole also forms microcoronas of pargasitic composition around garnet ("×" in Fig. 8c, d) and is particularly Al- and Ca-rich, with a high Fe^{2+} content (ID16: $X_{Fe^{2+}} = Fe^{2+}/(Fe^{2+} + Mn + Mg) = 0.429 \pm 0.029$ vs. 0.313 ± 0.017 for the matrix amphibole). These chemical characteristics are clearly related to the role of garnet as a reactant during the later amphibole growth, as is typical in the retrogression of eclogites worldwide.

In some samples, particularly ID33, some relict paragonite is surrounded by a corona of clinozoisite (Figs. 4d, S1d). We attempted to balance this coronitic reaction using the least-squares method (see Sect. 3):

$$0.516\mathrm{Pg} + 0.313\mathrm{Cam} + 1.358\mathrm{Qz} \rightarrow 1\mathrm{Czo} + 1.140\mathrm{Ab} + 0.067\mathrm{Kfs} + 0.844\mathrm{H_2O} + 1\boldsymbol{R},$$

where $\boldsymbol{R}$ is the residual vector ($Si_{0.000}$ $Al_{+0.002}$ $Ti_{-0.006}$ $Fe_{-0.081}$ $Mn_{+0.000}$ $Mg_{-0.774}$ $Ca_{+1.508}$ $Na_{-0.014}$ $K_{-0.002}$). Although at first glance the result fits the observation, the large residuals for Ca and Mg indicate that one or more other reactants, now consumed (omphacite?), may have been involved in the reaction or that the latter took place in an open system.

These garnet amphibolites show notable differences from the glaucophane eclogites: absence of omphacite, presence of Ca-rich amphibole instead of Na or Na–Ca amphiboles, and ubiquitous albite. However, they also show remarkable similarities: similar composition and zoning of garnet crystals; presence of paragonite, quartz and rutile (as relics within titanite coronas); and ferro-pargasite coronas around garnet. It therefore appears clear that the garnet amphibolites are retrogression products of the eclogites, which is also supported by the presence in some partially retrogressed eclogite samples (e.g. ID9) of similar late microstructures (pargasite coronas around garnet, amphibole + albite symplectites and titanite coronas around rutile).

4.2 Mica schists

The mica schists have a satiny grey appearance and alternate with levels rich in quartz. Under the polarising microscope, they are composed as follows (in order of decreasing abundance): quartz; white micas; garnet crystals that can reach a few millimetres in diameter; clinozoisite in small euhedral crystals; chlorite, which commonly forms small aggregates of several millimetres that appear as dark spots to the naked eye; albite, commonly interstitial; rutile surrounded by titanite coronas; rare tourmaline (dravite); and fluorapatite, monazite and zircon crystals of a few micrometres in size.

Table 2. Composition of amphiboles. avg(n): average composition of n analyses; $\pm 1\sigma$: standard deviation; *: calculated by stoichiometry; minimal values have been retained for Fe^{3+}. Nomenclature and the calculation procedure are taken from Hawthorne et al. (2012) and Locock (2014). Samples: glaucophane eclogites (ID1, ID9), eclogite layer (ID25a), garnet glaucophanite layer (ID25b) and retrogressed eclogites (ID16, ID33).

	Inclusions in garnet				Glaucophane nuclei in the matrix						Ca–Na-amphibole overgrowths in the matrix								Coronas around garnet										Rims of amphibole crystals				Late amphibole as symplectites with albite							
Sample	ID1		ID9		ID1		ID9		ID25b		ID1		ID9		ID25a		ID25b		ID1		ID9		ID16		ID25a		ID25b		ID1		ID25b		ID1		ID16		ID33			
wt %	avg(17)	±1σ	avg(2)	±1σ	avg(33)	±1σ	avg(16)	±1σ	avg(63)	±1σ	avg(260)	±1σ	avg(2)	±1σ	avg(9)	±1σ	avg(98)	±1σ	avg(13)	±1σ	avg(25)	±1σ	avg(18)	±1σ	avg(3)	±1σ	avg(3)	±1σ	avg(37)	±1σ	avg(29)	±1σ	avg(38)	±1σ	avg(36)	±1σ	avg(9)	±1σ		
SiO_2	40.09	0.542	55.91	0.089	56.52	0.946	56.66	1.098	57.94	1.100	50.20	2.574	49.62	1.286	48.62	0.360	48.41	2.420	44.14	3.167	43.72	3.636	44.09	1.493	45.51	1.680	38.55	0.541	51.60	2.404	49.16	1.638	51.84	1.628	48.78	1.795	48.21	0.729		
TiO_2	0.46	0.061	0.05	0.062	0.03	0.025	0.05	0.028	0.03	0.021	0.18	0.080	0.15	0.020	0.21	0.055	0.22	0.078	0.27	0.184	0.20	0.125	0.26	0.029	0.21	0.046	0.13	0.035	0.12	0.064	0.20	0.128	0.10	0.061	0.22	0.047	0.26	0.023		
Al_2O_3	17.54	1.068	11.55	0.717	11.22	0.286	10.89	0.427	11.60	0.411	9.15	2.198	9.45	0.280	12.00	0.550	12.77	1.460	13.92	2.853	15.52	3.162	14.58	1.342	12.61	1.383	19.40	0.250	5.62	2.329	5.14	2.327	6.44	1.642	9.61	1.913	10.31	0.781		
Cr_2O_3	0.03	0.035	0.00	0.000	0.02	0.021	0.00	0.000	0.03	0.035	0.02	0.032	0.00	0.000	0.01	0.011	0.02	0.030	0.03	0.031	0.00	0.000	0.02	0.025	0.01	0.014	0.00	0.000	0.03	0.041	0.02	0.026	0.01	0.016	0.03	0.030	0.03	0.034		
Fe_2O_3*	0.16	0.460	0.00	0.000	0.00	0.000	0.00	0.000	0.00	0.000	0.03	0.348	0.00	0.000	0.00	0.000	0.01	0.100	0.09	0.339	0.09	0.473	0.00	0.000	0.00	0.000	0.81	1.404	0.03	0.152	0.24	0.573	0.03	0.159	0.00	0.000	0.00	0.000		
FeO	18.81	0.869	13.39	0.450	10.63	0.736	11.52	0.618	8.91	1.096	13.37	2.353	13.69	1.848	14.12	0.285	14.21	1.945	17.78	2.089	17.30	2.263	14.34	0.672	16.58	1.024	21.11	0.942	12.91	2.891	19.11	0.679	12.02	1.419	11.81	0.705	15.34	0.364		
MnO	0.08	0.079	0.05	0.002	0.05	0.045	0.02	0.027	0.04	0.043	0.08	0.059	0.04	0.004	0.06	0.025	0.09	0.084	0.12	0.036	0.06	0.033	0.15	0.086	0.08	0.038	0.19	0.027	0.09	0.062	0.36	0.118	0.08	0.038	0.12	0.060	0.13	0.066		
MgO	6.78	0.202	8.77	0.248	10.78	0.603	10.12	0.379	11.44	0.517	12.47	1.957	11.91	0.939	10.73	0.303	10.31	0.697	8.56	1.924	7.66	2.131	10.43	0.726	9.55	0.480	4.11	0.945	14.36	2.317	10.37	0.727	14.94	1.396	13.95	1.164	11.07	0.516		
CaO	9.43	0.433	1.12	0.118	1.59	0.333	1.48	0.422	1.41	0.502	8.42	1.131	7.72	0.479	7.47	0.338	7.04	1.550	9.36	1.181	7.94	0.614	10.41	0.270	9.04	0.194	10.09	0.446	10.65	0.951	11.24	0.765	9.33	1.077	10.08	0.307	8.58	0.476		
Na_2O	4.05	0.315	7.09	0.333	6.86	0.432	6.77	0.221	6.78	0.278	3.30	0.774	3.97	0.044	4.34	0.196	4.39	0.873	3.19	0.958	4.42	0.327	2.67	0.386	3.50	0.451	2.07	1.286	1.78	0.748	1.23	0.578	2.72	0.700	2.41	0.249	2.73	0.226		
K_2O	0.16	0.074	0.02	0.005	0.03	0.017	0.03	0.020	0.03	0.019	0.16	0.058	0.23	0.003	0.07	0.044	0.13	0.081	0.24	0.187	0.42	0.149	0.74	0.168	0.11	0.083	0.49	0.238	0.07	0.046	0.16	0.054	0.13	0.045	0.32	0.134	0.28	0.027		
F	0.06	0.076	0.00	0.000	0.08	0.122	0.00	0.000	0.07	0.071	0.11	0.150	0.00	0.000	0.05	0.035	0.11	0.106	0.03	0.041	0.00	0.000	0.03	0.045	0.04	0.027	0.18	0.152	0.10	0.154	0.05	0.053	0.18	0.292	0.09	0.182	0.08	0.094		
Cl	0.38	0.203	0.00	0.000	0.00	0.008	0.00	0.000	0.01	0.007	0.02	0.023	0.00	0.000	0.00	0.000	0.06	0.066	0.00	0.000	0.00	0.000	0.05	0.038	0.00	0.000	0.54	0.312	0.02	0.029	0.04	0.068	0.00	0.000	0.01	0.024	0.02	0.011		
H_2O*	1.86	0.062	2.15	0.007	2.13	0.061	2.16	0.011	2.16	0.038	2.03	0.082	2.08	0.028	2.05	0.019	2.01	0.060	2.00	0.041	2.02	0.039	2.01	0.029	2.02	0.031	1.74	0.157	2.03	0.067	1.98	0.040	2.01	0.143	2.04	0.090	2.02	0.046		
O≡F,Cl	−0.11	0.050	0.00	0.000	−0.03	0.051	0.00	0.000	−0.03	0.031	−0.05	0.063	0.00	0.000	−0.02	0.016	−0.06	0.044	−0.01	0.018	0.00	0.000	−0.02	0.024	−0.02	0.015	−0.20	0.133	−0.05	0.064	−0.03	0.033	−0.07	0.123	−0.04	0.077	−0.04	0.039		
Total	99.84	0.543	100.09	0.266	99.96	0.698	99.69	0.457	100.50	0.592	99.54	0.702	98.85	0.289	99.72	0.407	99.78	0.715	99.76	1.028	99.37	0.423	99.83	0.565	99.25	0.080	99.37	0.335	99.43	0.725	99.31	0.620	99.76	0.420	99.46	0.481	99.10	0.290		
Name	ferro-pargasite		glaucophane		glaucophane		glaucophane		glaucophane		winchite		katophorite		katophorite		katophorite		ferro-pargasite		ferro-katophorite		pargasite		pargasite		ferro-sadanagaite		actinolite		ferro-actinolite		magnesio-hornblende		magnesio-hornblende		magnesio-hornblende			
Site T																																								
Si	6.059	0.0882	7.808	0.0262	7.814	0.0809	7.871	0.0922	7.877	0.0846	7.253	0.2606	7.238	0.1195	7.038	0.0541	6.999	0.2410	6.567	0.3493	6.510	0.4257	6.487	0.1702	6.754	0.2064	5.923	0.0500	7.466	0.2507	7.384	0.2245	7.433	0.1701	7.053	0.2130	7.081	0.0813		
Al	1.941	0.0882	0.193	0.0262	0.186	0.0809	0.129	0.0922	0.123	0.0846	0.747	0.2606	0.763	0.1195	0.962	0.0541	1.001	0.2410	1.433	0.3493	1.490	0.4257	1.513	0.1702	1.246	0.2064	2.077	0.0500	0.534	0.2507	0.616	0.2245	0.567	0.1701	0.947	0.2130	0.919	0.0813		
Site C																																								
Ti	0.053	0.0067	0.005	0.0071	0.003	0.0025	0.005	0.0030	0.003	0.0022	0.019	0.0090	0.017	0.0021	0.023	0.0060	0.024	0.0085	0.030	0.0208	0.022	0.0139	0.028	0.0033	0.023	0.0049	0.015	0.0044	0.013	0.0069	0.022	0.0145	0.011	0.0066	0.024	0.0051	0.028	0.0025		
Al	1.183	0.1160	1.708	0.0827	1.642	0.0837	1.655	0.0288	1.736	0.0606	0.815	0.2081	0.862	0.0559	1.085	0.0667	1.176	0.2021	1.015	0.2498	1.245	0.1917	1.016	0.1195	0.961	0.0704	1.436	0.0223	0.429	0.1836	0.295	0.1992	0.524	0.1671	0.693	0.1474	0.867	0.0941		
Cr	0.000	0.0000	0.000	0.0000	0.000	0.0000	0.000	0.0000	0.011	0.0116	0.000	0.0007	0.000	0.0000	0.001	0.0014	0.008	0.0101	0.000	0.0000	0.000	0.0000	0.010	0.0141	0.001	0.0017	0.111	0.1554	0.000	0.0003	0.010	0.0159	0.000	0.0000	0.006	0.0092	0.012	0.0119		
Fe^{3+}*	0.018	0.0522	0.000	0.0000	0.000	0.0000	0.000	0.0000	0.000	0.0000	0.003	0.0394	0.000	0.0000	0.000	0.0000	0.001	0.0114	0.011	0.0394	0.011	0.0534	0.000	0.0000	0.000	0.0000	0.000	0.0000	0.003	0.0176	0.027	0.0643	0.003	0.0175	0.000	0.0000	0.000	0.0000		
Fe^{2+}	2.209	0.0936	1.462	0.0156	1.126	0.0834	1.245	0.0776	0.932	0.1196	1.471	0.2979	1.532	0.2376	1.576	0.0219	1.569	0.2597	2.041	0.2335	2.026	0.3264	1.657	0.0824	1.903	0.1121	2.497	0.1065	1.453	0.3943	2.325	0.1003	1.269	0.2038	1.271	0.1024	1.669	0.0431		
Mg	1.528	0.0494	1.826	0.0601	2.223	0.1284	2.095	0.0661	2.318	0.0890	2.683	0.3897	2.590	0.1803	2.315	0.0672	2.222	0.1276	1.895	0.4066	1.696	0.4387	2.288	0.1508	2.112	0.0896	0.941	0.2160	3.092	0.4491	2.321	0.1574	3.193	0.2788	3.007	0.2397	2.424	0.1131		
Site B																																								
Mn^{2+}	0.016	0.0082	0.007	0.0007	0.008	0.0045	0.003	0.0033	0.004	0.0049	0.01	0.0065	0.005	0.0007	0.007	0.0032	0.012	0.0107	0.016	0.0047	0.008	0.0043	0.021	0.0088	0.011	0.0050	0.025	0.0036	0.012	0.0073	0.043	0.0165	0.010	0.0046	0.016	0.0065	0.016	0.0081		
Fe^{2+}	0.169	0.0411	0.102	0.0438	0.103	0.0360	0.094	0.0192	0.083	0.0272	0.15	0.0487	0.139	0.0042	0.134	0.0282	0.154	0.0431	0.179	0.1063	0.136	0.0349	0.108	0.0270	0.156	0.0376	0.216	0.0831	0.116	0.0488	0.076	0.0584	0.174	0.0423	0.158	0.0304	0.216	0.0372		
Ca	1.528	0.0774	0.167	0.0184	0.236	0.0502	0.220	0.0658	0.206	0.0756	1.31	0.1816	1.207	0.0863	1.159	0.0534	1.096	0.2598	1.496	0.2073	1.271	0.1192	1.642	0.0439	1.437	0.0299	1.661	0.0805	1.653	0.1612	1.809	0.1189	1.435	0.1753	1.562	0.0547	1.351	0.0792		
Na	0.293	0.0814	1.725	0.0622	1.654	0.0602	1.683	0.0719	1.707	0.0870	0.53	0.1863	0.650	0.0898	0.700	0.0541	0.746	0.2657	0.335	0.2346	0.585	0.1155	0.232	0.0562	0.397	0.0501	0.098	0.1114	0.220	0.1302	0.071	0.0783	0.391	0.1538	0.266	0.0646	0.418	0.0798		
Site A																																								
Na	0.893	0.0383	0.196	0.0191	0.185	0.1261	0.141	0.0405	0.082	0.0463	0.39	0.1498	0.474	0.0884	0.517	0.0450	0.488	0.1212	0.606	0.1217	0.694	0.1773	0.530	0.1167	0.612	0.1435	0.520	0.2794	0.279	0.1288	0.288	0.1043	0.375	0.0833	0.411	0.0791	0.359	0.0412		
K	0.030	0.0141	0.004	0.0014	0.005	0.0029	0.006	0.0038	0.006	0.0033	0.03	0.0108	0.043	0.0000	0.014	0.0082	0.023	0.0155	0.046	0.0369	0.081	0.0295	0.140	0.0324	0.022	0.0159	0.096	0.0473	0.014	0.0084	0.030	0.0103	0.023	0.0082	0.059	0.0253	0.052	0.0050		
ΣA	0.923	0.0431	0.200	0.0177	0.190	0.1270	0.146	0.0434	0.086	0.0487	0.42	0.1536	0.517	0.0884	0.530	0.0472	0.511	0.1226	0.652	0.1069	0.775	0.2004	0.670	0.1400	0.634	0.1518	0.616	0.2907	0.293	0.1328	0.318	0.1119	0.398	0.0870	0.469	0.0982	0.411	0.0394		
Site W																																								
OH	1.874	0.0559	2.000	0.0000	1.966	0.0533	2.000	0.0000	1.968	0.0308	1.95	0.0689	2.000	0.0000	1.975	0.0160	1.934	0.0481	1.987	0.0197	2.000	0.0000	1.973	0.0264	1.981	0.0127	1.772	0.1557	1.950	0.0680	1.968	0.0378	1.920	0.1322	1.955	0.0837	1.959	0.0427		
F	0.029	0.0365	0.000	0.0000	0.033	0.0534	0.000	0.0000	0.031	0.0307	0.05	0.0694	0.000	0.0000	0.025	0.0160	0.052	0.0482	0.013	0.0197	0.000	0.0000	0.016	0.0210	0.019	0.0127	0.086	0.0745	0.044	0.0694	0.022	0.0254	0.080	0.1322	0.042	0.0835	0.036	0.0436		
Cl	0.097	0.0525	0.000	0.0000	0.001	0.0019	0.000	0.0000	0.001	0.0016	0.00	0.0058	0.000	0.0000	0.000	0.0000	0.014	0.0168	0.000	0.0000	0.000	0.0000	0.012	0.0094	0.000	0.0000	0.142	0.0817	0.005	0.0074	0.010	0.0172	0.000	0.0000	0.002	0.0059	0.006	0.0027		
Σcations	15.923	0.0433	15.200	0.0184	15.190	0.1268	15.146	0.0435	15.086	0.0488	15.42	0.1535	15.516	0.0891	15.531	0.0479	15.511	0.1227	15.652	0.1066	15.775	0.2003	15.670	0.1399	15.634	0.1520	15.616	0.2899	15.293	0.1328	15.318	0.1120	15.398	0.087	15.469	0.0982	15.411	0.0392		

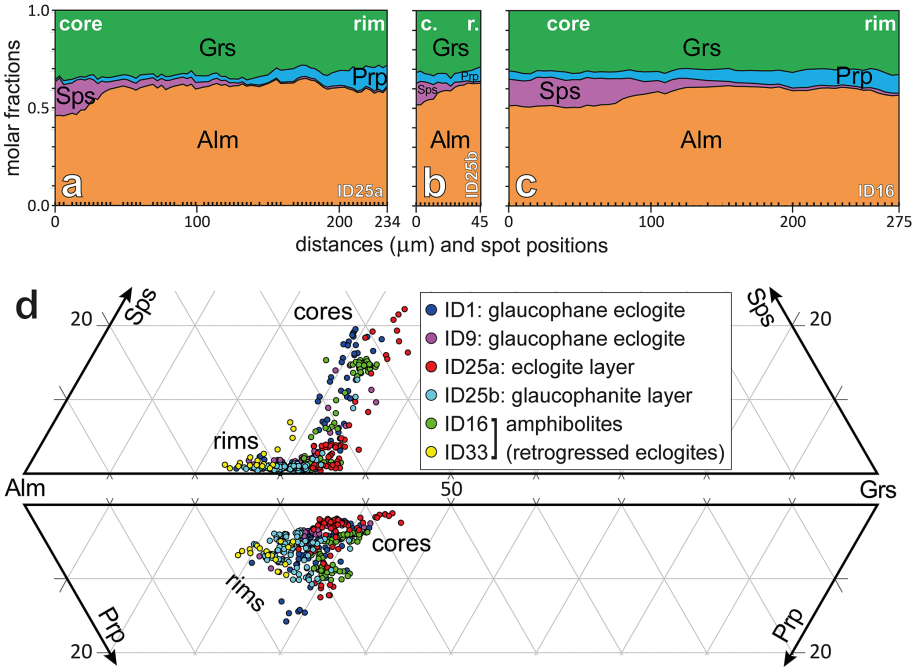

Figure 6. Garnet composition and zoning in metabasites. **(a–c)** Garnet zoning in the eclogite **(a)** and garnet glaucophanite **(b)** bands of sample ID25 and in the garnet amphibolite ID16 **(c)**. The analytical EMP spots are shown on the x axis; a few of these that touched inclusions in the garnet have been removed. **(d)** Barycentric plot of EMP analyses of garnet from the studied metabasites (mol % of spessartine, almandine, grossular and pyrope end-members). All four plots show more Mn in the cores and more Mg at the rims.

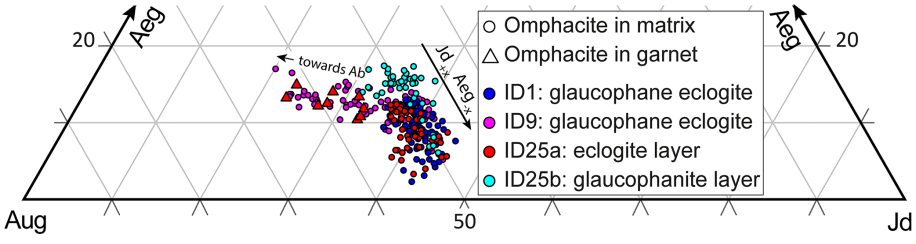

Figure 7. Omphacite composition in eclogites. Barycentric plot of EMP analyses of omphacite from the studied eclogites (mol % of jadeite, aegirine and other ("Aug") end-members). Triangles: early omphacite trapped in garnet; circles: omphacite in matrix. A slight scatter along the vector Jd_{+x} Aeg_{-x} is interpreted as being due to the uncertainty in the estimation of Fe^{3+}; on the other hand, the tendency for jadeite depletion in sample ID9 results from the partial exsolution of jadeite in the form of albite, present in this sample near the edges of the omphacite crystals ("towards Ab").

In sample ID13 (Figs. 4e, f, S1e), phengite is the dominant mica (Ms_{58} $FCel_7$ Cel_{23} Pg_{10} Mrg_1), with an average Si content of 6.573 ± 0.206 apfu. The large standard deviation of this value reflects a significant variation in the phengite substitution (Si_{+1} Al^{IV}_{-1} Al^{VI}_{-1} $(Mg, Fe)_{+1}$), which decreases towards the edge of the crystals (Fig. 4e, f). Paragonite (Pg_{90} Ms_8 $FCel_1$ Cel_0 Mrg_1) is inferred to be residual, as it occurs in the form of rare lamellae preserved in phengite flakes, whereas it is absent in the albite-rich matrix (Fig. 4e, f). Garnet forms small, slightly zoned infra-millimetre crystals (on average, Alm_{63} Grs_{24} Prp_8 Sps_4 Adr_1), with a core richer than the rim in Ca and Mn, reflecting typical prograde growth; in places, it is atoll-shaped with a "lagoon" of phengite and quartz (Fig. 4e). Chlorite crystals generally form multi-millimetre radiating clusters (Fig. 4f), suggesting that they replaced an earlier mineral, such as biotite or chloritoid; the chlorite is a clinochlore with $X_{Mg} = 0.586 \pm 0.020$ and $Si = 2.745 \pm 0.070$ apfu. Subhedral microcrystals of clinozoisite ($X_{Fe^{3+}} = 0.119 \pm 0.006$) and titanite characteristically enveloping relics of rutile (Fig. 4e, f) are common.

4.3 Orthogneiss

The gneiss of the southern part of the island is a fairly homogeneous, equigranular and leucocratic rock with an average millimetric grain size. It shows strong foliation and less pronounced stretching lineation. Sample ID17 (Figs. 4g,

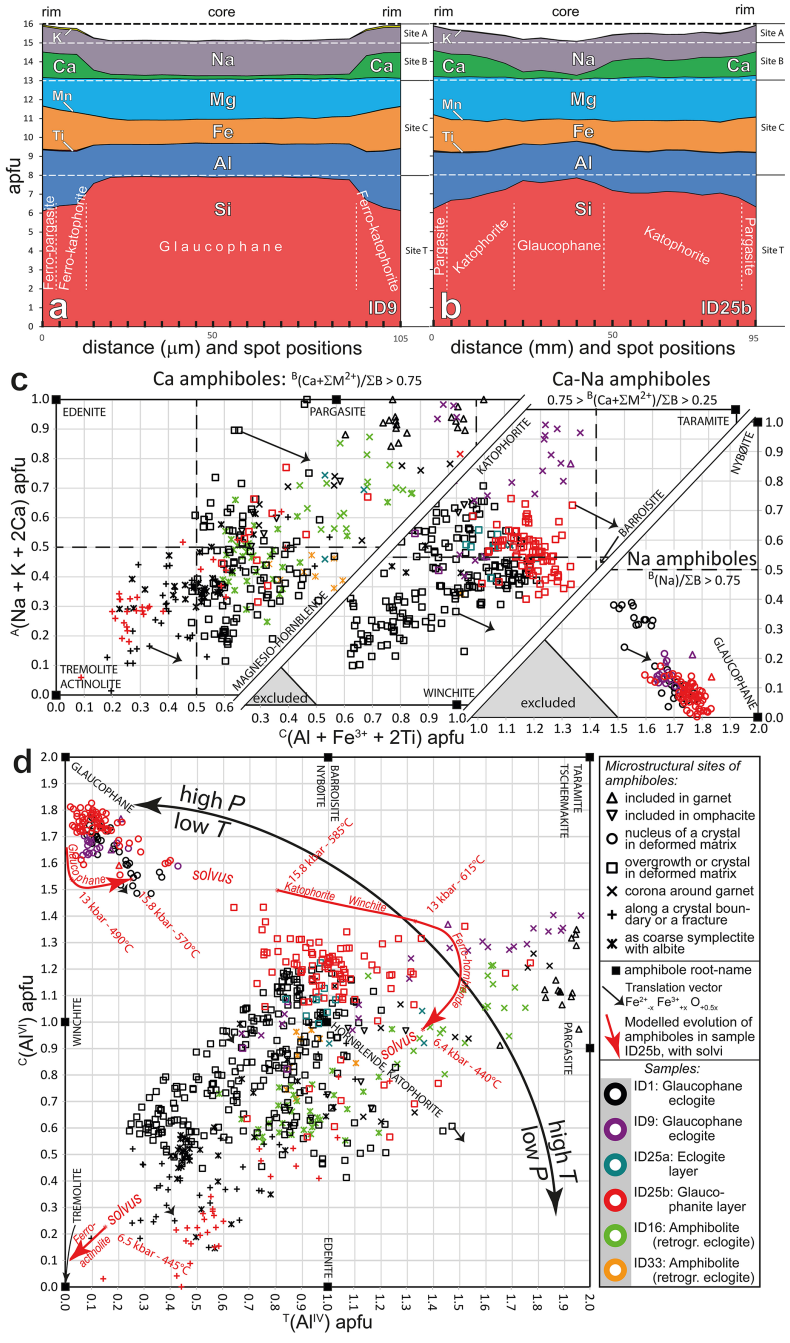

Figure 8. Amphibole composition and zoning in metabasites. **(a, b)** Zoning of two amphibole crystals with a glaucophane nucleus and overgrowths of (ferro-)katophorite to (ferro-)pargasite, from garnet glaucophanite ID9 **(a)** and ID25b **(b)**. The EMP analytical spots are shown on the x axis. **(c)** EMP analyses of amphibole in the classification diagrams of Hawthorne et al. (2012); the three plots of Site A vs. Site C are at different levels (> 0.75, intermediate, < 0.25) along the axis of Site B, best imagined as perpendicular to the plots; the selected segments of the first two plots overlap. **(d)** The same amphibole analyses in the Al^{VI}–Al^{IV} diagram, where the $(Al^{VI} / (Al^{VI} + Al^{IV}))$ isopleths radiate from their origin at "tremolite" and are correlated with the predicted P/T ratio, which decreases clockwise (represented by the curved black arrow), thus showing the effect of P and T on the amphibole composition; red arrows: theoretical evolution of the amphiboles in sample ID25b along the P–T path of Fig. 9b, following the solid-solution model of Green et al. (2016) (see text). For **(c)** and **(d)**, the colour indicates the sample provenance and the symbol style indicates the microstructural location (see the incorporated legend). The $Fe^{2+}_{-x}Fe^{3+}_{+x}O_{+0.5x}$ vector shows, for some analyses, the translation that occurs when the estimated value of Fe^{3+} goes from 0 to $0.1 \times Fe_{tot}$. The names in capital letters are the amphibole "root names" (e.g. "PARGASITE"), which actually consist of several end-member species (e.g. ferro-pargasite and pargasite); all glaucophanes have $X_{Mg} > 0.5$, and most of the other clinoamphiboles have $X_{Mg} < 0.5$ and therefore take the prefix "ferro-".

S1f) belongs to a leucocratic facies, rich in white mica and poor in biotite, located near the contact with mica schists. Its main minerals are quartz and phengite (Ms_{60} Fe^{3+}–Ms_7 $FCel_{24}$ Cel_6 Pg_2 Mrg_1) with an average Si content of 6.695 ± 0.076 apfu, microcline ($Or_{94.0}$ $Ab_{5.5}$ $An_{0.0}$ $Cls_{0.5}$), and albite ($Or_{0.6}$ $Ab_{99.0}$ $An_{0.4}$ $Cls_{0.0}$). The feldspars show exsolution lamellae of K-feldspar in the albite (i.e. antiperthite) and, less commonly, of albite in the microcline (i.e. perthite; Fig. 4g), which also frequently shows the Carlsbad twin. Some aggregates, less than a millimetre in size, are formed of chlorite + garnet ± phengite ± K-feldspar + iron oxide (Fig. 4h). The chlorite is a chamosite with $X_{Mg} = 0.062$ to 0.068 and Si = 5.9 to 6.3 apfu; it shows a significant amount of potassium (1.2 wt % to 2.0 wt % K_2O), suggesting that it is derived from the breakdown of former biotite. The garnet in these aggregates is concentrated at their margins, particularly near plagioclase grains, but without forming regular coronas (Fig. 4h). It has a peculiar Ca-rich composition ($Grs_{58.8 \pm 1.4}$ $Alm_{34.0 \pm 1.7}$ $Adr_{6.3 \pm 2.1}$ $Sps_{0.7 \pm 0.4}$ $Prp_{0.1 \pm 0.0}$) and may contain a small amount of hydrogarnet (Si = 2.980 ± 0.017 apfu). Monazite, fluorapatite and zircon are accessory minerals.

5 Discussion

5.1 Evidence for high-pressure blueschist-facies metamorphism at Dumet Island

5.1.1 Eclogite and garnet glaucophanite

The P–T pseudosections calculated for the eclogite and garnet glaucophanite bands of sample ID25 (Fig. 9a and b, respectively) make it possible to unravel the metamorphic history of this sample by combining the stability field of the different parageneses observed and the most significant isopleths (see Sect. 3 for the method). Isopleths depending on Fe^{3+}, either directly ($X_{Fe^{3+}}$ in epidote) or indirectly ($X_{Fe^{2+}}$ in omphacite), were discarded as too uncertain, since they depend both on the value assigned to the extra amount of O linked to Fe^{3+} in the modelled bulk-rock composition and on the imprecise estimation of Fe^{3+} in the minerals by stoichiometry. To specify the P–T evolution of sample ID25, we have therefore used the isopleths of omphacite and garnet (Fig. 9c, d), which we present here with the uncertainty interval of $\pm 1\sigma$ that results from the EMP analyses of the minerals. Other sources of uncertainty are difficult to quantify and therefore cannot be taken into account, such as those related to the thermodynamic data or to the bulk-rock composition; Palin et al. (2016) attempted to assess these uncertainties, which they estimated to be of the order of ± 1 kbar and ± 50 °C.

Three successive parageneses were investigated in this way, in each of the two levels of sample ID25.

a. The first paragenesis consists of the core of the garnet crystals and their inclusions; it gives information on the prograde metamorphism. The P–T co-stability field of these inclusions (titanite, Jd-poor omphacite, epidote, quartz, etc.) with their host garnet is outlined in blue in Fig. 9c–d. The X_{Fe} and X_{Mn} isopleths of the garnet, as well as the X_{Na} of some early omphacite trapped in garnet of eclogite ID25a (triangles in Fig. 7), allow us to constrain the P–T conditions of this stage. However, the interpretation of these results is complicated by several difficulties: the inclusions were probably not all trapped at the same time, certain elements (Mn, Ca) were fractionated during garnet growth, the garnet may have undergone a late partial chemical homogenisation, etc. Perhaps these problems may explain why the Ca-in-garnet isopleth for both rocks gave P–T conditions slightly outside the stability fields of this paragenesis. Despite these difficulties, one interesting feature should be noted: the isopleths marking the growth of the garnet core are shifted to lower-grade and earlier blueschist-facies conditions in eclogite ID25a compared to glaucophanite ID25b, where the modelled modal amount of garnet (not shown) increases only late, near the peak, in the Gln–Grt–Ep–Chl–Qz–Ttn field (Fig. 9b), probably explaining the relatively small size of the garnet crystals in this glaucophanite level (see Fig. 6b vs. 6a).

b. The second paragenesis is formed by the matrix minerals in contact with the rims of the garnet crystals; it allows the assessment of the P–T conditions at the peak of metamorphism. The Mn-in-garnet isopleth, with very low values ($X_{Mn} \approx 0.01$), is of no help here, as it gives large intervals covering almost the entire stability domain of the paragenesis, outlined in red in Fig. 9c–d; again, the Ca-in-garnet isopleth gave P–T conditions slightly outside the stability domain of sample ID25a. For both samples, the stability domain of the main paragenesis, combined with the isopleths, gives conditions of the order of 16 kbar and 620 °C, for the P and T peaks, respectively (Fig. 9).

c. The third paragenesis consists of the later retrograde minerals (actinolite, albite, chlorite, titanite, etc.), which appeared in the form of microcoronas or symplectites at the expense of the second paragenesis. Its stability domain within the greenschist facies (framed in green in Fig. 9c–d) allows us to set a milestone on the retrograde path and confers a clockwise shape to the whole P–T path.

5.1.2 Amphibole evolution in the garnet glaucophanite

While modelling the P–T pseudosections, we have not used amphibole isopleths (X_{Fe}, X_{NaA}, X_{NaM4}, etc.) because of the complexity and therefore the low reliability of the available solid-solution models, the impossibility of accurately evalu-

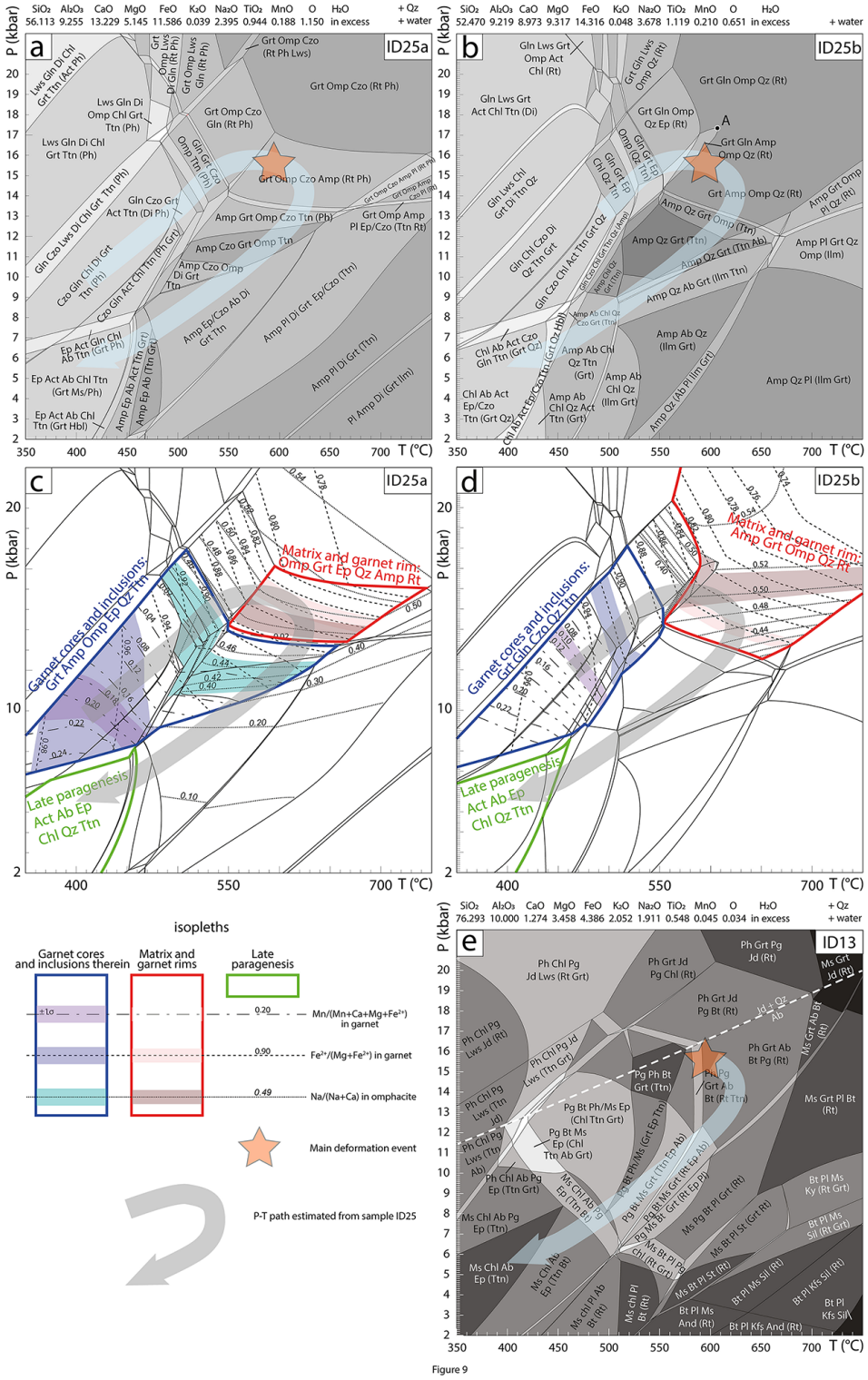

Figure 9

Figure 9. *P–T* pseudosections. **(a, c)** Pseudosection **(a)** and isopleths **(c)** for the epidote-rich eclogite band (sample ID25a). **(b, d)** Pseudosection **(b)** and isopleths **(d)** for the garnet–glaucophanite band (sample ID25b); A: apex of the solvus between glaucophane (Gln) + Ca–Na amphibole (Amp) (see text). **(e)** Pseudosection for mica schist (sample ID13). The minerals are listed in decreasing order of abundance, the ones in brackets being of negligible quantity (< 2 vol %). The Ab = Jd + Qz univariant curve is plotted in **(e)** to show the extension of the stability domain of albite (see Sect. 5.4). The thick curved grey arrow is the *P–T* trajectory derived from the modelling of sample ID25. The orange star indicates the main deformation event.

ating Fe^{3+} in amphibole (see Sect. 3), and also the great variability in the composition of amphiboles depending on their microstructural position in the rock (Fig. 8). Nevertheless, the modelling of sample ID25b gives interesting indications regarding the evolution of amphiboles in the garnet glaucophanites of Île Dumet. The solid-solution model of Green et al. (2016) considers three types of amphiboles, namely a glaucophane, a (ferro-)actinolite, and finally a Ca or Ca–Na amphibole – which we have named "Amp" in the pseudosections, although the THERMOCALC package calls it "hb", since in our case it is not strictly speaking a hornblende. The chemical evolution of these amphiboles along the P–T trajectory has been modelled for sample ID25b and is shown in the diagram in Fig. 8d (red arrows). This confirms that glaucophane "Gln" was formed during the prograde path, while Na–Ca amphibole "Amp" (katophorite/winchite) appeared near the T peak, with more katophorite than winchite components in the higher-T conditions. Between Gln and Amp, the model predicts a solvus, which is indeed clearly manifested by the presence of a gap in the composition of the amphiboles (Fig. 8c, d) and by a sharp transition in the amphibole crystals between the glaucophane nuclei and the katophorite/winchite overgrowths (Gln and kw, respectively, in Fig. 4b). The rock ID25b should have evolved within the P–T space through this Gln–Amp solvus (i.e. through the Grt Gln Amp Omp Qz Rt ± Ep fields of Fig. 9b) and therefore below the solvus apex (point A in Fig. 9b), at $P < 17.3$ kbar and $T < 607$ °C; otherwise the transition between the two amphiboles would have been gradual. The model also suggests another miscibility gap between Ca amphibole (Amp) and ferro-actinolite (Act); although less obvious, this Amp–Act solvus is also manifested for sample ID25b by a lower density of analytical points in the composition diagrams (between the red squares and red plusses in Fig. 8c, d), as well as by a sharp transition between katophorite/winchite and ferro-actinolite, which commonly forms a thin but contrasting border at the edge of the crystals ("Act" in Fig. 4b).

The evolution of the amphiboles results in a global clockwise trajectory in the Al^{VI}–Al^{IV} diagram (Fig. 8d), which mimics the clockwise trajectory of the rocks in the P–T diagram (Fig. 9b, d): since Al in the tetrahedral site of the silicates is favoured by T and hindered by P, the Al^{VI} / Al^{IV} ratio is indeed roughly correlated with the P/T ratio (e.g. Smith, 1988).

Katophorite/winchite overgrowths on glaucophane nuclei are oriented parallel to the foliation (Fig. 4b). This indicates the existence of an important episode of plastic deformation, mainly by diffusion creep of the amphibole crystals, under P–T conditions close to the Gln–Amp transition (see above) and therefore close to the peak (orange stars in Fig. 9). This tectonic episode could reflect a more global geodynamic event that led to the end of subduction and the beginning of exhumation. Whatever the cause, this deformation contributed to the transposition parallel to the foliation of the centimetre-scale banding observed in the glaucophane eclogites (i.e. samples ID1, ID9, ID25). Even if it can be partially inherited from a magmatic layering, this banding seems to be largely elaborated by mineral segregation during metamorphism, since each type of band, eclogitic and glaucophanitic, corresponds to normative compositions of incompatible magmatic rocks, oversaturated with labradorite and undersaturated with andesite, respectively (Table 1). Incidentally, Smith (1988) argued for "mechanical segregation" into bands that produced peculiar bulk-rock compositions in some Norwegian eclogites. The rare-earth-element (REE) profile normalised to chondrites is similar in both cases (Fig. 5) but with a slight enrichment of REEs for eclogite bands relative to those rich in glaucophane. This difference can be explained by the abundance of epidote in eclogite levels, as epidotes are known to readily fix light REEs in the form of allanite and/or dissakisite end-members in solid solution, especially in eclogites and glaucophanites (Gieré and Sorensen, 2004, p. 461). The affinity of Eu for Ca-bearing minerals, including epidote, may also explain the slightly positive Eu anomaly of the eclogite band, symmetrical to the slightly negative anomaly of the glaucophane band.

5.1.3 Mica schists

The last P–T pseudosection (Fig. 9e) shows the retrograde evolution of mica schist sample ID33, taken near the metabasite lenses on the north of the island (see Sect. 4.2). The HP paragenesis, composed of phengite, quartz, garnet, rutile, biotite and paragonite, has undergone large retrograde changes, notably a decrease in phengitic substitution at the margins of the white mica flakes, the disappearance of paragonite which remains only as isolated lamellae in phengite, the development of albite (Ab_{98}) and the formation of chlorite (Fig. 4e, f; Sect. 4.2). The pseudosection suggests that chlorite was formed here from biotite, whereas elsewhere in the Vilaine estuary and on the island of Groix, it generally developed at the expense of chloritoid (see below). All these changes agree reasonably well with the retrograde P–T path derived from the glaucophane eclogite ID25 (Fig. 9).

5.2 The Dumet Island and the Vilaine estuary: the equivalent of Groix Island

The HP metamorphic rocks of Dumet Island show striking analogies with those of Groix Island and the Bois-de-Céné region, where glaucophane-bearing rocks are also boudinaged within phengite-bearing mica schists. As Dumet Island is isolated in the Vilaine estuary, it is difficult to examine its geological relationships with the mainland. However, several geological formations outcropping on the north and south banks of the Vilaine estuary are similar to those of Dumet, Groix and Bois-de-Céné, as summarised here:

a. The best-preserved *metabasite lenses* on Dumet Island are similar to some glaucophane eclogites on Groix Island. They have undergone a comparable P–T his-

tory but with a higher P gradient at Groix, as suggested by the lower T at the metamorphic peak (about 520 °C at Groix (Bosse et al., 2002) vs. 620 °C at Dumet (Fig. 9)) and the presence of lawsonite at Groix (e.g. Ballèvre et al., 2003), whereas only epidote has been observed at Dumet. They also show several generations of amphiboles, sodic (glaucophane), sodic–calcic (katophorite, winchite) and finally calcic (magnesiohornblende, actinolite), recalling an evolution already observed in the amphiboles of Groix and Bois-de-Céné (Triboulet, 1978, 1991).

Metabasite lenses can also be observed around the Vilaine estuary (e.g. 47.4248, −2.4561; 47.4411, −2.4809; 47.5115, −2.5490; 47.5104, −2.5540; 47.5217, −2.7095). They are fine-grained foliated rocks composed of millimetre-sized crystals of albite, epidote, chlorite, Ca-rich clinoamphibole, almandine–grossular-rich garnet crystals partly transformed into Fe-rich chlorite along cracks and rims, and titanite possibly containing relics of rutile and/or ilmenite. These rocks are strongly modified by greenschist-facies metamorphism, and no researcher has reported eclogite- or blueschist-facies relics in them. However, glaucophane has been observed in the form of detrital grains in Quaternary and Cenozoic sediments of the Vilaine estuary and its banks (Fig. 10b), at Pointe du Touru near Mesquer, together with rutile (Chauris, 1997), at Pénestin, in association with chloritoid and kyanite (Durand and Milon, 1955; Durand, 1960), and on the estuarine seabed (Bouysse, 1966a, b). Benjamin Rondeau (personal communication, 2022) also observed loose blocks of retrogressed eclogite on the shore at Piriac.

b. Although quite rare, (pluri)hectometric lenses of *serpentinite* can be found in the mica schists, both on the island of Groix (47.6531, −3.4927) and in the Bois-de-Céné region (46.9478, −1.8519; 46.9480, −1.8489; 46.9553, −1.8406; 46.9417, −1.7583; 46.9414, −1.7603). We did not observe any on Dumet Island, whose size is rather limited, but there are some indications of their presence elsewhere in the Vilaine estuary. Chromite and, incidentally, olivine have been reported in coastal sands at Cromenach and Bétahon, near Damgan (Fig. 10b; Chauris, 1982). Fuchsite was also reported by Baret (1898, p. 124) between Piriac and Mesquer, in the former La Roche Bleue quarry.

c. On the island of Groix and in the Bois-de-Céné region, metabasites and serpentinites are boudinaged within *phengite ± chloritoid + garnet mica schists*, which are the dominant rock type (e.g. Bosse et al., 2002). Chloritoid was not observed at Dumet. However, chloritoid-bearing mica schists are quite common elsewhere in the Vilaine estuary, where they were first described by Barrois (1884), who related them to the mica schists of the island of Groix, and then by Lacroix (1893–1910, vol. 1, pp. 368, 391), who noted the frequent transformation of chloritoid into chlorite. Later, chloritoid was observed on the right bank of the estuary, on the Rhuys peninsula (Rollando, 1951, 1952), in particular at Grand Mont, Kervoyal, Penvins and Damgan (e.g. 47.4916, −2.6821; Fig. 10b), as well as on the left bank, NW of the Guérande peninsula (Audren, 1974; Audren et al., 1975). Phengite and minor paragonite are also quite common in some mica schists of the Rhuys peninsula (e.g. Augier et al., 2010), notably at Kervoyal where we sampled and studied a mica schist (47.5114, −2.5536) similar to, but apparently less retrogressed than, those of Dumet Island (e.g. ID13); it consists of quartz, phengite (Ms_{37} Cel_{22} $FCel_{18}$ Pg_{11} Mrg_1; Si $= 6.650 \pm 0.146$ apfu), garnet ($Alm_{72.3\pm3.47}$ $Gr_{13.2\pm3.48}$ $Prp_{6.1\pm0.50}$ $Sps_{8.4\pm0.74}$), chlorite ($X_{Mg} = 0.392 \pm 0.051$), paragonite (Pg_{90} Ms_5 Mrg_2 $FCel_2$ $Ti\text{-}Ph_1$), ilmenite, minor rutile and some albite formed during retrogression.

d. A few *Mn-rich quartzite lenses* (quartz + spessartine ± piedmontite), 0.1 to 1 m in size, have been reported within the mica schists at Groix (e.g. Lacroix, 1888; Guy Cornen, personal communication, 2020) and Bois-de-Céné (Godard in Lahondère et al., 2009, p. 44). They are still unknown in the Vilaine estuary, where their discovery would strengthen the analogy with Groix.

e. Levels of *orthogneiss*, 0.1 to 1 m thick, are intercalated in the mica schists of the east coast of Groix, at Les Sables Rouges (Fig. S2; El Korh et al., 2012). They show structural and petrological similarities with the orthogneiss of Dumet Island (compare Figs. 3b and S2), where it is nevertheless much more abundant. The latter is also petrographically similar to that of Pénestin (Audren, 1974), located on the banks of the Vilaine estuary, about 12 km NE of Dumet Island (Fig. 10). Finally, some orthogneiss has also been observed at Bois-de-Céné, where it is very poorly exposed (Godard in Lahondère et al., 2009, p. 45).

These indices indicate that the blueschist-facies Groix Unit is present not only on Dumet Island, but also on the banks of the estuary where, however, the metabasites have been completely retrogressed into greenschist-facies metabasite. On the map in Fig. 10, we have drawn this formation so as to include the various phengite and chloritoid occurrences in the mica schists, assuming boundaries subparallel to the schistosity strike.

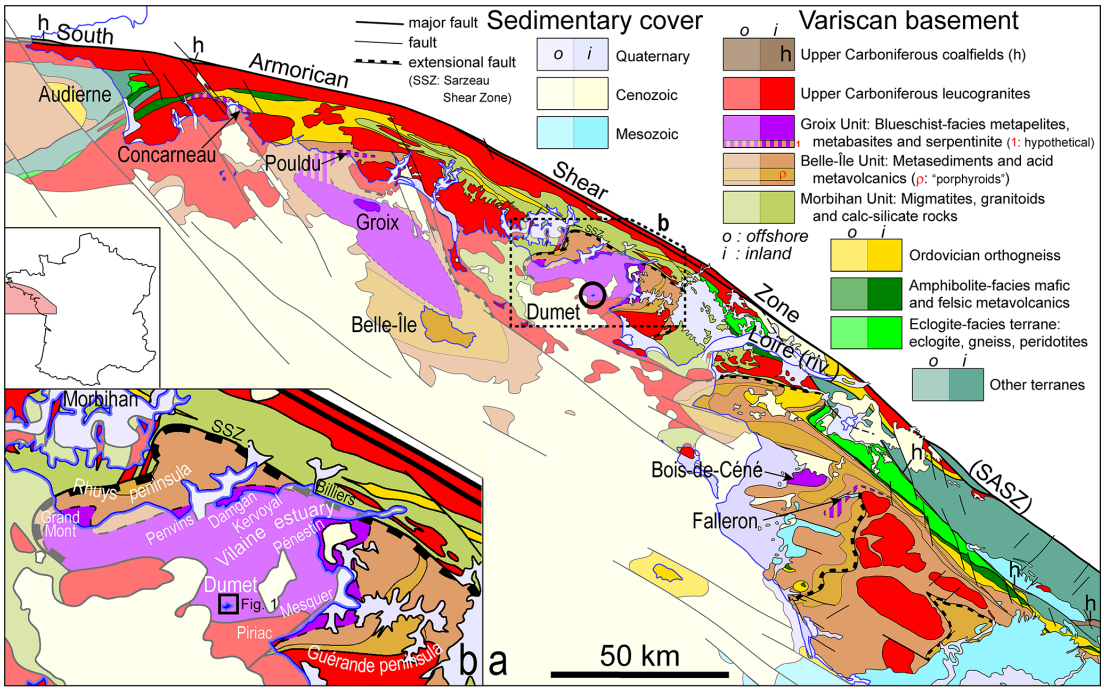

Figure 10. Dumet Island in the South Armorican context. Sketch geological maps of the South Armorican Domain **(a)** and the Vilaine estuary **(b)**, based on existing geological maps at 1 / 50 000 and unpublished surveys. SSZ: Sarzeau Shear Zone. Geological formations are represented by light and dark shades of colour where they are located offshore (o) and inland (i), respectively.

5.3 Dumet Island in the South Armorican tectonic stack

The "Groix Unit", at both Groix and Bois-de-Céné, has been interpreted as two klippen in the core of synformal structures, at the top of a tectonic stack showing a general flat-lying planar fabric with a WNW–ESE stretching lineation, largely disturbed by upper Carboniferous tectonics and granitic intrusions (e.g. Audren, 1990; Gapais et al., 1993; Burg et al., 1994; Le Hébel et al., 2002a; Turrillot et al., 2011). In interpreting Dumet Island and the western part of the Vilaine estuary as the geological equivalent of Groix Island, it is necessary to verify whether the same structural framework applies there. Below, we review the main subdivisions recognised in this stack from bottom to top and discuss whether they also occur in the Vilaine estuary:

a. *Morbihan migmatite unit.* At the base of the stack, cordierite and sillimanite migmatites derived from metapelites are intruded by anatectic granitoids (Audren and Le Métour, 1976; Brown, 1983; Audren, 1987; Jones and Brown, 1989, 1990; Audren and Triboulet, 1993; Brown and Dallmeyer, 1996; Marchildon and Brown, 2003; Johnson and Brown, 2004; Augier et al., 2010). These migmatites contain decametre-thick metasedimentary layers composed of banded calc-silicate rocks, little studied since Charles Barrois (1887, 1897) and Alfred Lacroix (1889, 1891) and whose mineralogy is reminiscent of that of skarns, with diopside, hornblende; plagioclase; epidote; scapolite; grossular-rich garnet; titanite; and, incidentally, calcite, vesuvianite, wollastonite and scheelite. *P–T* estimation of peak metamorphic conditions gave 8–10 kbar and 750–800 °C for the migmatites of this unit (Jones and Brown, 1989, 1990).

This lower unit is well known in the Gulf of Morbihan, to the NW of the Vilaine estuary, and is also well exposed to the SE, on both banks of the Loire estuary, in the regions of Saint-Nazaire and Saint-Brévin (e.g. Lacroix, 1889, 1891; Fig. 10). To the NE, it occupies the upstream part of the Vilaine estuary (Fig. 10b), where banded calc-silicate rocks with diopside, amphibole, epidote and grossular (Billiers, Pen Lan, Tréhiguier) occur within biotite + sillimanite mica schists and migmatitic gneisses (e.g. Audren, 1974, pp. 3-6); these calc-silicate rocks have long been confused with the metabasites of the downstream part of the estuary, which we now attribute to the HP Groix Unit (see below). The metasedimentary origin of the calc-silicate rocks is attested by some cipolin remnants (Coëtsurho, near Billiers: e.g. Barrois, 1897, p. 28; Audren, 1974; Audren et al., 1975), as is the case near Saint-Nazaire and Saint-Brévin further south (Lacroix, 1889, 1891). They are associated with amphibolites to which Triboulet and Audren (1985a, b) attributed a volcanic de-

trital origin but whose unusually high Ca content (Triboulet and Audren, 1985c, p. 61) confirms a strong sedimentary carbonate supply.

The Morbihan migmatite unit is commonly roofed by major gently dipping extensional shear zones (e.g. "Sarzeau Shear Zone": SSZ in Fig. 10a, b) along which leucogranite laccoliths were emplaced during shearing (Gapais et al., 1993; Turrillot et al., 2009, 2011). Northeast of the Vilaine estuary, the steeply dipping SE extension of the sinistral SSZ separates the Morbihan and Belle-Île/Saint-Gilles units.

b. *Belle-Île/Saint-Gilles Unit.* Metasediments, consisting mainly of mica schists with numerous intercalations of graphite-rich quartzite and acid metavolcanics known as "porphyroids", tectonically overlie the Morbihan Unit (e.g. Audren and Jégouzo, 1986; Audren, 1987; Le Hébel et al., 2002b; Augier et al., 2010). The metamorphic grade increases downwards from chlorite + albite greenschist-facies to garnet ± staurolite + biotite amphibolite-facies conditions (e.g. Triboulet and Audren, 1988; Goujou, 1992; Brown and Dallmeyer, 1996). *P*–*T* estimates gave peak conditions of 7–9 kbar and 350–400 °C (Le Hébel et al., 2002b). The so-called "porphyroids" (i.e. metavolcanics) were dated to the Ordovician (Ballèvre et al., 2012).

This intermediate unit has been termed the "lower allochthon" by Ballèvre et al. (2014). It is well represented on the island of Belle-Île and on the Rhuys and Guérande peninsulas on either side of the Vilaine estuary, as well as south of the Loire River, around the Bois-de-Céné klippe, where it has been named the "Saint-Gilles Unit" (e.g. Lahondère et al., 2009).

c. *Groix Unit*. The well-known HP Groix Unit, described above (see Sect. 5.2) and attributed to the oceanic "middle allochthon" by Ballèvre et al. (2014), is located in the core of synformal folds, at Groix, at Bois-de-Céné and thus in the Vilaine estuary (Fig. 10). This last occurrence has hitherto gone unnoticed because the metabasites of the western part of the Vilaine estuary, which we here assign to the Groix Unit (see Sect. 5.2, item a), have been confused with the calc-silicate rocks of the NE part of the estuary, which belong to the Morbihan Unit (see above). Although difficult to distinguish due to strong retrogression, Morbihan-type calc-silicate rocks and Groix-type metabasites can be discriminated on the basis of their mineralogy, which includes relics of skarn-like high-*T* assemblages in the former and of HP metamorphic parageneses in the latter.

The contact of the various Groix-type klippen with the underlying Belle-Île/Saint-Gilles Unit, mainly located at sea, seems to have been observed in only one place, in the Bois-de-Céné klippe (46.9346, −1.760). The transition between the two units there is gradual, with concordant schistosity and lineation, suggesting that the tectonic juxtaposition of the two units was syn-metamorphic (Rebay and Godard, in Lahondère et al., 2009). Such a syn-metamorphic ductile fault has also been demonstrated by Bosse et al. (2002) on the island of Groix, within the Groix Unit itself.

There are other geological formations in the South Armorican Domain, particularly at its outer edge near the South Armorican Shear Zone (SASZ in Fig. 10a), where they are strongly stretched and verticalised. They are not considered here, but it is useful to mention an eclogite-facies formation, large occurrences of which are preserved in Galicia in Spain (Cabo Ortegal), in Finistère in France (Bay of Audierne) and south of the Loire (Les Essarts Unit). Although this last formation testifies to HP eclogite-facies metamorphism, it is clearly distinct from the Groix Unit by its petrology and tectonometamorphic evolution (e.g. Godard, 1988, 2009; Ballèvre et al., 2009, 2014); it has been attributed to the upper allochthon by Ballèvre et al. (2014).

5.4 Multiple occurrences of Groix-type unit in the Ibero-Armorican Arc

The progressive and tectonically concordant contact between the Groix and Belle-Île/Saint-Gilles units, combined with the very general retrogression in the greenschist facies of the Groix-type metabasites, explains why the Groix Unit has not yet been recognised within the synformal fold of the Vilaine estuary, of which Île Dumet is the centre. For the same reasons, other remnants of the same formation may have gone unnoticed. To identify them, it is necessary to combine structural criteria (e.g. klippe over the Belle-Île/Saint-Gilles Unit) with petrological data (presence of garnet + phengite ± paragonite ± chloritoid mica schists, with possible lenses of serpentinite and glaucophanite more or less retrogressed). In the following, we examine the various regions, from the west (Iberia) to the east (French Massif Central), where these criteria seem to apply:

a. Arenas et al. (2021) present solid evidence for the integration of the very distant Badajoz–Córdoba Unit (SW Iberian Massif) into the blueschist-facies belt of the Ibero-Armorican Arc, on the basis of its petrology, age and metamorphic conditions (Devonian blueschist-facies metamorphism). Correlations with such distant formations, probably still hypothetical, are undoubtedly a stimulating research objective for the future.

b. In the Iberian part of the Ibero-Armorican Arc, some occurrences of glaucophanite and glaucophane–chloritoid-bearing metapelites occur in the Trás-os-Montes region of northern Portugal (e.g. Gil Ibarguchi and Dallmeyer, 1991) and in the Ceán Unit of Galicia (e.g. Lopez-Carmona et al., 2014; Arenas et al., 2016).

c. West of Concarneau (northern Brittany; Fig. 10a), some rocks of the "Nerly group", including mica schists, ultramafites (Kerlévot) and metabasites (Béchennec and Hallégouët, 1999), could be assigned to the Groix Unit if one accepts an extreme retrogression in greenschist-facies conditions. In the same region, coastal sands from the southern part of the Bay of Audierne gave Chauris (1992) a relatively large number of glaucophane grains, suggesting the presence of glaucophanite at sea.

d. Near Le Pouldu, between Concarneau and Lorient (Fig. 10a), metabasites with blue-green "subglaucophanic actinote" were studied by Triboulet (1980, 1992); they are associated in the field with garnet and chloritoid mica schists (Triboulet, 1983; Béchennec et al., 2012). Although the metamorphic conditions here do not strictly belong to the blueschist facies, Triboulet insisted on the similarity of the evolution of these rocks with those of Groix, both for the metabasites (Triboulet, 1980, p. 99) and for the metapelites (Triboulet, 1983, p. 203).

e. The blueschist-facies rocks of the island of Groix have been extensively studied since their discovery in 1883 (e.g. Audren et al., 1993; Ballèvre et al., 2003, and references therein; see historical review in Godard, 2019). Although largely masked by the ocean, they have also been observed at Baz Moullek, 11 km SE of Groix Island, where submarine cores have yielded chloritoid mica schists and glaucophane metabasites (Delanoë et al., 1972), and extend up to 35 km SE of Groix, between the island of Belle-Île and the Quiberon peninsula (Audren and Jégouzo, 1986).

f. The western Vilaine estuary and Dumet Island constitute another klippe, described here.

g. South of the Loire, the Bois-de-Céné Formation (Fig. 10a) forms the core of a synform bounded by "porphyroids" of the Belle-Île Unit (also known there as the Saint-Gilles Unit). It includes glaucophanites and serpentinites boudinaged within mica schists with garnet, phengite and chloritoid (Anthonioz and Brillanceau, 1969; Guiraud et al., 1987; Triboulet, 1991; Lahondère et al., 2009). Mg-rich chlorite schists associated with serpentinite at Bois-de-Céné yielded a protolith age identical to that of similar rocks from Île de Groix (U–Pb zircon: 488.8 ± 2.7 vs. 492.7 ± 3.2 Ma; Paquette et al., 2017).

h. Another synform of mica schists surrounded by "porphyroids" occurs in the Falleron area, about 10 km SE of Bois-de-Céné (Fig. 10a). Outcrop conditions there are very poor, and no glaucophanite has been reported. However, abundant glaucophane was observed in the alluvial deposits of local streams and rivers by Guigues and Devismes (1969) and also in local Cretaceous sandy sediments where it was observed together with garnet, epidote and chloritoid (Louail, 1984, pp. 234, 263). Guigues and Devismes (1969) reported another occurrence of alluvial glaucophane further to the SE, between La Ferrière and Les Essarts, where the Groix-type unit could be strongly stretched together with "porphyroids" of the Belle-Île/Saint-Gilles Unit.

i. Towards the SE, on the SW border of the French Massif Central, the Najac–Carmaux klippe with its glaucophane eclogites (Delor et al., 1986; Lotout et al., 2018), serpentinites and phengite + chloritoid + garnet mica schists (Delor et al., 1987; Quenardel et al., 1991) may belong to the same HP belt.

These multiple occurrences, some of which are hypothetical or poorly exposed, show that the Groix Unit exists in the Ibero-Armorican Arc in locations other than on the island of Groix and in the Bois-de-Céné region. They form a discontinuous belt of blueschist-facies metamorphism, which actually extends well outside the Armorican Massif. The origin and geodynamic evolution of this HP belt, discussed by many authors with particular reference to the island of Groix, are beyond the scope of this study. The mélange of pelitic metasediments, metabasites, serpentinites and Mn-rich quartzites, the latter being quite typical of an oceanic environment (e.g. Tumiati et al., 2010), suggests subduction of an oceanic accretionary prism (see discussion in Ballèvre et al., 2009, 2013, 2014) during the Upper Devonian (370–360 Ma: Bosse et al., 2005). According to Ballèvre et al. (2014), this oceanic unit would be part of the middle allochthon of the Ibero-Armorican Arc, but these authors also include in this tectonic domain some units (e.g. Drain, Saint-Martin-des-Noyers) that lack blueschist-facies metamorphism and whose metabasites largely dominate over metapelites so that, although oceanic, they probably have a different origin from that of the above-mentioned occurrences of the Groix Unit.

5.5 The embarrassing question of the Ordovician orthogneisses

The presence of orthogneisses within the Groix Unit, whether on Groix Island (Sables Rouges), in the Vilaine estuary (Dumet Island and Pénestin) or in the Bois-de-Céné region (see Sects. 4.3 and 5.2, item e), raises two difficult questions.

First, from a geodynamic point of view, it is difficult to explain the presence of metagranitoids in an environment interpreted as a subducting oceanic accretionary prism. On the island of Groix, El Korh et al. (2012) circumvented the problem by suggesting that the Sables Rouges orthogneiss was derived from acid volcanics rather than from a granitoid. This is more difficult to sustain for Dumet Island, given the numerous veins and apophyses of the orthogneiss stretched in mica schists and the enclaves of mica schists within

the orthogneiss (Figs. 1 and 3b), suggesting intrusion of a magmatic protolith. Furthermore, the presence of perthitic and antiperthitic exsolution lamellae in the feldspars of the Dumet Island orthogneiss (see Sect. 4.5) strongly favours a metagranitic origin.

The main problem is the degree of metamorphism of the orthogneisses, which do not seem to have undergone the HP conditions observed in the neighbouring glaucophane eclogites and still detected in the surrounding phengite + paragonite + garnet mica schists despite their retrogression. Admittedly, the white mica of the Dumet orthogneiss is phengite, with a significant celadonite substitution (see Sect. 4.3), and its biotite in contact with plagioclase has been partly replaced by aggregates composed of microgarnets, phengite and K-feldspar (Fig. 4h), reminiscent of the coronitic reactions that occur in metagranites and metapelites metamorphosed under eclogite-facies conditions, such as at Monte Mucrone in the Alps or in the surrounding gneisses of some Armorican eclogites (e.g. Godard, 2009; Gyomlai et al., 2023). However, doubts about the intensity of the HP metamorphism experienced by the Dumet orthogneiss are raised by the abundance of preserved K-feldspar and plagioclase apparently inherited from the magmatic protolith, as indicated at Dumet by perthitic and antiperthitic exsolution lamellae (sample ID17; Fig. 4g). K-feldspar generally survives HP metamorphism, but albite-rich plagioclase is predicted to transform into jadeite-bearing pseudomorphs (e.g. Gilotti et al., 2023). At Groix Island, plagioclase porphyroclasts also appear to be of magmatic origin, as they show albite and Carlsbad twins (Fig. 4 in El Korh et al., 2012), the latter being normally absent from metamorphic feldspars.

The absence of well-defined traces of HP metamorphism in the orthogneiss could be explained by an intrusion of the granitic protolith during the retrograde evolution of the surrounding HP rocks, before the last penetrative deformation (phase S2 of Audren, 1987). However, this hypothesis is contradicted at Groix by the Early Ordovician age attributed to the protolith of the orthogneiss (481.1 ± 3.7 Ma: El Korh et al., 2012), which pre-dates the age of the HP metamorphism (360–370 Ma: Bosse et al., 2005). Although no comparable geochronological data are available for Dumet Island, the imprecise but "old" Rb–Sr age of the orthogneiss (419 ± 12 Ma: Peucat, 1983) suggests an identical conclusion.

It is difficult to explain the survival of magmatic feldspars under blueschist- or eclogite-facies conditions, especially albitic plagioclase, which should disappear beyond the univariant P–T curve albite = jadeite + quartz (dashed line in Fig. 9e), which may have been exceeded by the nearby glaucophane eclogites at Dumet and more certainly at Groix, where the rocks have reached the lawsonite stability domain. However, there is some debate about the metastability of feldspars in the eclogite facies under anhydrous conditions. In particular, Austrheim (1987) argued for the metastable preservation of "dry" undeformed granulite-facies parageneses in the anorthosites of the Bergen Arcs (Norway), which in contrast are transformed into eclogites within shear zones under eclogite-facies conditions. Smith (1995, p. 320–321) referred to this hypothesis as the "ultrametastability model" since Al^{IV} in plagioclase should have been transformed to Al^{VI} at high P (see also the trend in Fig. 8d). He suggested that there may have been some "overpressure" in the shear zones that provided enough "extra" pressure to create the eclogites (Smith, 1988, 1995); it can also be admitted that the influx of fluid (Austrheim, 1987) and the deformation in the shear zones favoured the diffusion and hence the phase transitions. This debate has continued in more recent papers, such as that of Gyomlai et al. (2023) on the eclogite-facies metagranite of La Picherais in the Armorican Massif. Therefore, the metastability model could indeed solve the orthogneiss problem on the islands of Groix and Dumet.

6 Conclusions

Dumet Island contains numerous metre-sized lenses of metabasite revealing relict garnet glaucophanite and glaucophane eclogite, boudinaged within garnet- and phengite-bearing mica schists. Highly retrogressed metabasites and similar mica schists also occur on the mainland, on the banks of the Vilaine estuary. The whole of the Dumet Island geological formation is analogous to the well-known blueschist-facies formation of the island of Groix.

The best-preserved metabasites contain garnet, omphacite (Jd_{35-45}), quartz, clinoamphibole, epidote, and minor paragonite and rutile. Peak metamorphic conditions, modelled by the P–T pseudosection method, reached 16 kbar and 620 °C. The clinoamphibole crystals display a zoning from glaucophane at the P peak through katophorite/winchite to magnesio-hornblende/pargasite and finally to actinolite, accompanied by decreasing X_{Mg}. The evolution along this trend corresponds to a decrease in the $Al^{VI} / (Al^{VI} + Al^{IV})$ ratio in clinoamphibole due to increasing T and/or decreasing P along a clockwise P–T path, ending with widespread growth of late albite and calcic amphibole. The peak P of the metamorphism coincides with the main phase of ductile deformation, which resulted in katophorite/winchite overgrowths along the foliation direction from pre-existing glaucophane nuclei.

The host mica schists, composed of quartz, phengite with lamellae of paragonite, zoned garnet, chlorite, clinozoisite and titanite with remnants of rutile, have been largely affected by the retrograde metamorphism responsible for the formation of albite. On the mainland, they also contain chloritoid in some localities. They are analogous to the mica schists of the island of Groix.

An orthogneiss crops out on the southern part of the Dumet Island, as well as in the region of Pénestin on the mainland. Despite subsequent deformation, this metagranitoid still shows intrusive relationships with the mica schists. However, it has not developed clear traces of HP metamorphism,

apart from a few irregular garnet reaction coronas. In particular, magmatic feldspars seem to have been metastably preserved at higher P than some feldspar-out reactions. This orthogneiss appears to be an equivalent to that described at Les Sables Rouges on the island of Groix. The origin, age and metamorphic history of these orthogneisses, both at Groix and at Dumet, are the main problems to be solved for future research.

Île Dumet, together with the western part of the Vilaine estuary, is definitely considered in this article the "little sister" of the well-known Île de Groix. The blueschist-facies rocks of both islands belong to the Groix Unit, which is located at the top of the tectonic pile of the South Armorican Domain. About 10 similar occurrences of this HP unit have been preserved in the core of various synforms throughout the Ibero-Armorican Arc, but most of them have remained unnoticed until now due to the general retrogression of the rocks within the greenschist facies and their tectonic concordance with the underlying Belle-Île/Saint-Gilles Unit. This growing family of occurrences forms a discontinuous belt created by the subduction of an oceanic accretionary prism, at the beginning of the Variscan orogeny.

Code availability. The freeware (PCalc2.4) used to balance reactions and perform modal calculations and projections can be downloaded from the ResearchGate platform (https://www.researchgate.net/ (last access: 12 January 2024); https://doi.org/10.13140/RG.2.2.17290.03527, Godard, 2024).

Data availability. All the structural data are visualised in Fig. 1. Most of the analytical data are presented in Tables 1 and 2 and in the Supplement. The thermodynamic data are those of Holland and Powell (2011).

Supplement. The supplement related to this article is available online at: https://doi.org/10.5194/ejm-36-99-2024-supplement.

Author contributions. Field survey and sampling: GG, DS, DJ; SEM observation and EMP analyses: GG, DS, DJ; bulk rock analyses: DJ; mineralogical and petrological studies: GG, DS; pseudosection modelling: SD, GG; redaction and editing of text, figures and tables : GG, DS; improvement and corrections: GG, DS, DJ, SD.

Competing interests. The contact author has declared that none of the authors has any competing interests.

Disclaimer. Publisher's note: Copernicus Publications remains neutral with regard to jurisdictional claims made in the text, published maps, institutional affiliations, or any other geographical representation in this paper. While Copernicus Publications makes every effort to include appropriate place names, the final responsibility lies with the authors.

Special issue statement. This article is part of the special issue "(Ultra)high-pressure metamorphism, from crystal to orogenic scale". It is a result of the 14th International Eclogite Conference (IEC-14) held in Paris and Lyon, France, 10–13 July 2022.

Acknowledgements. We thank the Conservatoire de l'espace littoral et des rivages lacustres, in particular Odile Gauthier and Jean-Michel Laloue, for allowing us access to Île Dumet (convention no. 44-275). Our sincere thanks go to Michel Garnier, Daniel Eloi and Christian Piot, who volunteered to take us by boat from Piriac, thus facilitating our access to the island. Bernard Lasnier kindly provided us with thin sections of his rock samples from Dumet Island. We are grateful to Ricardo Arenas and Michel Ballèvre for their helpful reviews of the manuscript and to Samuel Angiboust and Christian Chopin for their editorial assistance. We dedicate this article to the memory of Claude Audren, who carried out the first detailed geological study of Île Dumet.

Review statement. This paper was edited by Samuel Angiboust and reviewed by Michel Ballèvre and Ricardo Arenas.

References

Affholder, J.-G.: Une nouvelle détermination du pôle des terres émergées, Le Monde des cartes: revue du Comité français de cartographie, 173–174, 43–58, 2002.

Anthonioz, P. M. and Brillanceau, A.: Introduction à la géologie de la région de Bois-de-Céné (Vendée); un nouveau jalon du métamorphisme de haute pression dans le massif Armoricain, C. R. Acad. Sci. Paris (Série D), 269, 1050–1052, https://gallica.bnf.fr/ark:/12148/bpt6k63251842/f226.item (last access: 12 January 2024), 1969.

Arenas, R., Sánchez Martínez, S., Díez Fernández, R., Gerdes, A., Abati, J., Fernández-Suárez, J., Andonaegui, P., González Cuadra, P., López Carmona, A., Albert, R., Manuel Fuenlabrada, J., and Rubio Pascual, F. J.: Allochthonous terranes involved in the Variscan suture of NW Iberia: A review of their origin and tectonothermal evolution, Earth-Sci. Rev., 161, 140–178, https://doi.org/10.1016/j.earscirev.2016.08.010, 2016.

Arenas, R., Novo-Fernández, I., Garcia-Casco, A., Díez Fernández, R., Fuenlabrada, J. M., Pereira, M. F., Abati, J., Sánchez Martínez, S., and Rubio Pascual, F. J.: A unique blueschist facies metapelite with Mg-rich chloritoid from the Badajoz-Córdoba Unit (SW Iberian Massif): correlation of Late Devonian high-pressure belts along the Variscan Orogen, Int. Geol. Rev., 63, 1634–1657, https://doi.org/10.1080/00206814.2020.1789509, 2021.

Audren, C.: Les schistes cristallins de la Vilaine (Bretagne méridionale), Bull. Soc. Géol. Minéral. Bretagne, 6, 1–41, 1974.

Audren, C.: Evolution structurale de la Bretagne méridionale au Paléozoïque, Mémoires Soc. Géol. Minéral. Bretagne, 31, 365 pp. + dépl., 1987.

Audren, C.: Evolution tectonique et métamorphique de la chaîne varisque en Bretagne méridionale, Schweiz. Mineral. Petrogr., 70, 17–34, 1990.

Audren, C. and Jégouzo, P.: Carte géologique de la France à 1/50 000, feuille Belle-Île-en-mer, îles Houat et Hoëdic (no 477), BRGM, Orléans, 1986.

Audren, C. and Le Métour, J.: Mobilisation anatectique et déformation. Un exemple: Les migmatites du Golfe du Morbihan (Bretagne méridionale), Bull. Soc. Géol. France, 9, 1041–1049, 1976.

Audren, C. and Triboulet, C.: P-T-t-deformation paths recorded by kinzigites during diapirism in the western Variscan belt (Golfe du Morbihan, southern Brittany, France), J. Metamorph. Geol., 11, 337–356, https://doi.org/10.1111/j.1525-1314.1993.tb00152.x, 1993.

Audren, C., Jégouzo, P., Barbaroux, L., and Bouysse, P.: Carte géologique de la France à 1/50 000, feuille La Roche-Bernard (no. 449), BRGM, Orléans, 1975.

Audren, C., Triboulet, C., Chauris, L., Lefort, J.-P., Vigneresse, J.-L., Audrain, J., Thiéblemont, D., Goyallon, J., Jégouzo, P., Guennoc, P., Augris, C., and Carn, A.: Carte géologique de la France, feuille Île de Groix à 1/25000, BRGM, Orléans, ISBN 2-7159-1415-6, 1993.

Augier, R., Turrillot, P., Van Vliet-Lanoë, B., Hallegouët, B., Menier, D., and Thinon, I.: Carte géologique de la France à 1/50 000, feuille Vannes Saint-Gildas-de-Rhuys (no. 417), BRGM, Orléans, ISBN 978-2-7159-1417-9, 2010.

Austrheim, H.: Eclogitization of lower crustal granulites by fluid migration in shear zones, Earth Planet. Sc. Lett., 81, 221–232, https://doi.org/10.1016/0012-821X(87)90158-0, 1987.

Ballèvre, M., Pitra, P., and Bohn, M.: Lawsonite growth in the epidote blueschists from the Ile de Groix (Armorican massif, France): a potential geobarometer, J. Metamorph. Geol., 21, 723–735, https://doi.org/10.1046/j.1525-1314.2003.00474.x, 2003.

Ballèvre, M., Bosse, V., Ducassou, C., and Pitra, P.: Palaeozoic history of the Armorican Massif: Models for the tectonic evolution of the suture zones, C. R. Géosci., 341, 174–201, https://doi.org/10.1016/j.crte.2008.11.009, 2009.

Ballèvre, M., Fourcade, S., Capdevila, R., Peucat, J.-J., Cocherie, A., and Mark Fanning, C.: Geochronology and geochemistry of Ordovician felsic volcanism in the Southern Armorican Massif (Variscan belt, France): Implications for the breakup of Gondwana, Gondwana Res., 21, 1019–1036, https://doi.org/10.1016/j.gr.2011.07.030, 2012.

Ballèvre, M., Bosse, V., Dabard, M.-P., Ducassou, C., Fourcade, S., Paquette, J.-L., Peucat, J.-J., and Pitra, P.: Histoire Géologique du massif Armoricain: Actualité de la recherche, Bull. Soc. Géol. Minéral. Bretagne, 10–11, 5–96, 2013.

Ballèvre, M., Martínez Catalán, J. R., López-Carmona, A., Pitra, P., Abati, J., Díez Fernández, R., Ducassou, C., Arenas, R., Bosse, V., Castiñeiras, P., Fernández-Suárez, J., Barreiro, J. G., Paquette, J.-L., Peucat, J.-J., Poujol, M., Ruffet, G., and Sánchez Martínez, S.: Correlation of the nappe stack in the Ibero-Armorican arc across the Bay of Biscay: a joint French–Spanish project, in: The Variscan Orogeny: Extent, timescale and the formation of the European crust, edited by: Schulmann, K., Martínez Catalán, J. R., Lardeaux, J. M., Janoušek, V., and Oggiano, G., Geological Society Special Publications, 405, 77–113, https://doi.org/10.1144/SP405.13, 2014.

Baret, C.: Minéralogie de la Loire-Inférieure, Bull. Soc. Sci. Nat. Ouest France, VIII, 1–175 + 119 pl., https://gallica.bnf.fr/ark:/12148/bpt6k1125075 (last access: 12 January 2024), 1898.

Barrois, C.: Note sur le chloritoïde du Morbihan, Bull. Soc. Minéral. France, VII, 37–43, https://doi.org/10.3406/bulmi.1884.1849, 1884.

Barrois, C.: Les pyroxénites des îles du Morbihan, Annales Soc. Géol. du Nord, XV, 69–96, https://gallica.bnf.fr/ark:/12148/bpt6k57244478 (last access: 12 January 2024), 1887.

Barrois, C.: Carte géologique de la France au 1/80 000, Feuille Quiberon (no. 103), Service géologique national, Paris, 1897.

Baudouin, J., Bodeur, Y., and Lasnier, B.: Géologie de l'Ile Dumet (Loire-Atlantique, France), Bull. Soc. Sci. Nat. Ouest France, 10, 109–134, 1988.

Béchennec, F. and Hallégouët, B.: Carte géologique de la France (1/50 000), feuille Quimper (346) + Notice explicative par Béchennec, F., Hallégouët, B., Thiéblemont, D., avec la collaboration de Guerrot, C., Cocherie, A., et Carn, A., BRGM, Orléans, 161 pp., ISBN 2-7159-1346-X, 1999.

Béchennec, F., Hallégouët, B., and Thinon, I.: Carte géologique de la France (1/50 000), feuille Lorient (383) + Notice explicative par Béchennec, F., Hallégouët, B., Thiéblemont, D., Thinon, I., avec la collaboration de Cocherie, A., Guerrot, C., et Lucassou, F., BRGM, Orléans, 206 pp., ISBN 978 2 7159 1383 7, 2012.

Berget, A.: Répartition géographique des Océans (détermination du pôle continental), Annales Institut océanographique, 5, 1–12, 1913.

Bosse, V., Ballèvre, M., and Vidal, O.: Ductile thrusting recorded by the garnet isograd from blueschist-facies metapelites of the Île de Groix, Armorican massif, France, J. Petrol., 43, 485–510, https://doi.org/10.1093/petrology/43.3.485, 2002.

Bosse, V., Féraud, G., Ballèvre, M., Peucat, J.-J., and Corsini, M.: Rb-Sr and $^{40}Ar/^{39}Ar$ ages in blueschists from the Île-de-Groix (Armorican Massif, France): Implications for closure mechanisms in isotopic systems, Chem. Geol., 220, 21–45, https://doi.org/10.1016/j.chemgeo.2005.02.019, 2005.

Bouysse, P.: Recherches du B.R.G.M. sur le plateau continental; A, Résultats généraux obtenus par les premières campagnes du "Beluga" en Baie de la Vilaine et ses abords, Bull. B.R.G.M., Section 2: Géologie Appliquée, Chronique des Mines, 5, 3–17, 1966a.

Bouysse, P.: La baie de la Vilaine; étude sédimentologique et morphologique, Cahiers Océanographiques, 18, 319–341, 1966b.

Brown, M.: The petrogenesis of some migmatites from the Presqu'île de Rhuys, southern Brittany, France, in: Migmatites, Melting and Metamorphism, edited by: Atherton, M.-P., and Gribble, C.-D., Shiva Publishing, Nantwich, 174–200, ISBN 13 978 0906812266, 1983.

Brown, M. and Dallmeyer, R. D.: Rapid Variscan exhumation and the role of magma in core complex formation: southern Brittany metamorphic belt, France, J. Metamorp. Geol., 14, 361–379, https://doi.org/10.1111/j.1525-1314.1996.00361.x, 1996.

Burg, J. P., Van Den Driessche, J., and Brun, J.-P.: Syn-to post-thickening extension: mode and consequences, C. R. Acad. Sci. Paris (Série 2), 319, 1019–1032, 1994.

Chauris, L.: Les sables lourds des plages du Mor Bras – Introduction à l'étude des placers littoraux en Bretagne méridionale, Bull. Soc. Sci. Nat. Ouest France, 4, 1–58, 1982.

Chauris, L.: Contribution à l'étude du littoral de la baie d'Audierne (Finistère), Nature et origine des minéraux lourds des plages, Norois, 39, 451–458, 1992.

Chauris, L.: Paragenèse des sables lourds à cassitérite de la Baie de la Vilaine (Massif Armoricain), Bull. Soc. Sci. Nat. Ouest France, 19, 1–13, 1997.

Delanoë, Y., Gallenne, B., Lasnier, B., and Pinot, J.-P.: Découverte par carottage sous-marin d'une association pétrographique de micaschistes à chloritoïde et de schistes verts à glaucophane autour de la Baz Moullek, à 11 km au Sud-Est de l'île de Groix (Morbihan), C. R. Acad. Sci. Paris (Série D), 274, 644–646, https://gallica.bnf.fr/ark:/12148/bpt6k5748432m/f766.item (last access: 12 January 2024), 1972.

Delor, C., Bodinier, J.-L., and Burg, J.-P.: Découverte d'éclogites à glaucophane dans la klippe de Najac (Massif Central, France); nouveaux témoins océaniques d'un stade haute pression dans la chaine de collision varisque, C. R. Acad. Sci. Paris (Série 2), 302, 739–744, https://gallica.bnf.fr/ark:/12148/bpt6k6296984t/f753.item (last access: 12 January 2024), 1986.

Delor, C., Burg, J. P., Guiraud, M., and Leyreloup, A.: Les métapélites à phengite-chloritoïde-grenat-staurotide-disthène de la klippe de Najac-Carmaux: Nouveaux marqueurs d'un métamorphisme de haute pression varisque en Rouergue occidental, C. R. Acad. Sci. Paris (Série 2), 305, 589–595, https://gallica.bnf.fr/ark:/12148/bpt6k63051247/f603.item (last access: 12 January 2024), 1987.

Delorme, P.: L'île aux chimères, Éditions du Trésor, Paris, 60 pp., ISBN 979 10 91534 60 4 (br.), 2020.

Díez Fernández, R., Arenas, R., Pereira, M. F., Sánchez Martínez, S., Albert, R., Martín Parra, L.-M., Rubio Pascual, F. J., and Matas, J.: Tectonic evolution of Variscan Iberia: Gondwana–Laurussia collision revisited, Earth-Sci. Rev., 162, 269–292, 2016.

Dresch, J.: Note sur l'île Dumet (Loire-Atlantique), Norois, 11, 39–41, 1964.

Durand, S.: Le tertiaire de Bretagne. Etude stratigraphique, sédimentologique et tectonique, Mémoires Soc. Géol. minéral. Bretagne, 12, 390 pp., 1960.

Durand, S. and Milon, Y.: Le pliocène de l'estuaire de la Vilaine; étude des falaises de Pénestin (Morbihan), Bull. Soc. Géol. Minéral. Bretagne, 1955, 1–15 + 15 pl., 1955.

El Korh, A., Schmidt, S. T., Ballèvre, M., Ulianov, A., and Bruguier, O.: Discovery of an albite gneiss from the Ile de Groix (Armorican Massif, France): geochemistry and LA-ICP-MS U–Pb geochronology of its Ordovician protolith, Int. J. Earth Sci. (Geol. Rundsch.), 101, 1169–1190, https://doi.org/10.1007/s00531-011-0732-5, 2012.

Evensen, N. M., Hamilton, P. J., and O'Nions, R. K.: Rare-earth abundances in chondritic meteorites, Geochim. Cosmochim. Ac., 42, 1199–1212, https://doi.org/10.1016/0016-7037(78)90114-X, 1978.

Gapais, D., Lagarde, J.-L., Le Corre, C., Audren, C., Jégouzo, P., Casas Sainz, A., and van Den Driessche, J.: La zone de cisaillement de Quiberon: témoin d'extension de la chaîne varisque en Bretagne méridionale au Carbonifère, C. R. Acad. Sci. Paris (Série 2), 316, 1123–1129, https://gallica.bnf.fr/ark:/12148/bpt6k6316609v/f145.item (last access: 12 January 2024), 1993.

Gieré, R. and Sorensen, S. S.: Allanite and other REE-rich epidote-group minerals, in: Epidotes, edited by: Liebscher, A., and Franz, G., Reviews in Mineralogy and Geochemistry, Mineralogical Society of America, Washington, DC, vol. 56, 431–493, https://doi.org/10.2138/gsrmg.56.1.431, 2004.

Gil Ibarguchi, J. I. and Dallmeyer, R. D.: Hercynian blueschist metamorphism in North Portugal: tectonothermal implications., J. Metamorph. Geol., 9, 539–549, https://doi.org/10.1111/j.1525-1314.1991.tb00547.x, 1991.

Gilotti, J. A., McClelland, W. C., Schorn, S., Compagnoni, R., and Coble, M. A.: Provenance, protolith and metamorphic ages of jadeite-bearing orthogneiss and host paragneiss at Tavagnasco, the Sesia Zone, Lower Aosta Valley, Italy, Eur. J. Mineral., 35, 645–658, https://doi.org/10.5194/ejm-35-645-2023, 2023.

Godard, G.: Petrology of some eclogites in the Hercynides: the eclogites from the southern Armorican massif, France, in: Eclogites and Eclogite-Facies Rocks, edited by: Smith, D. C., Developments in Petrology 12, Elsevier, Amsterdam, 451–519, ISBN 13 978 0444430304, 1988.

Godard, G.: Two orogenic cycles recorded in eclogite-facies gneiss from the Southern Armorican Massif (France), Eur. J. Mineral., 21, 1173–1190, https://doi.org/10.1127/0935-1221/2009/0021-1984, 2009.

Godard, G.: La découverte de la glaucophane à Groix en 1883: histoire d'une mystification, Bull. Soc. Géol. Minéral. Bretagne, 17, 31–56, ISSN 1774-0991, 2019.

Godard, G.: PCalc2.4, ResearchGate [code], https://doi.org/10.13140/RG.2.2.17290.03527, 2024.

Goujou, J.-C.: Analyse pétro-structurale dans un avant-pays métamorphique; influence du plutonisme tardi-orogénique varisque sur l'encaissant épi à mésozonal de Vendée, Documents du B.R.G.M., 216, 347 pp., ISBN 2 7159 0541 6 (br.), 1992.

Green, E. C. R., White, R. W., Diener, J. F. A., Powell, R., Holland, T. J. B., and Palin, R. M.: Activity-composition relations for the calculation of partial melting equilibria in metabasic rocks, J. Metamorp. Geol., 34, 845–869, https://doi.org/10.1111/jmg.12211, 2016.

Guigues, J. and Devismes, P.: La prospection minière à la batée dans le Massif armoricain, Mémoires du B.R.G.M., 71, 171 pp., 1969.

Guiraud, M., Burg, J.-P., and Powell, R.: Evidence for a variscan suture zone in the Vendée, France: a petrological study of blueschist facies rocks from Bois de Cené, J. Metamorph. Geol., 5, 225–237, 1987.

Gyomlai, T., Yamato, P., and Godard, G.: Petrological study of an eclogite-facies metagranite from the Champtoceaux Complex (La Picherais, Armorican Massif, France), Eur. J. Mineral., 35, 589–611, https://doi.org/10.5194/ejm-35-589-2023, 2023.

Hawthorne, F. C., Oberti, R., Harlow, G. E., Maresch, W. V., Martin, R. F., Schumacher, J. C., and Welch, M. D.: Nomenclature of the amphibole supergroup, Am. Mineral.t, 97, 2031–2048, https://doi.org/10.2138/am.2012.4276, 2012.

Holland, T. J. B. and Powell, R.: Activity-composition relations for phases in petrological calculations: an asymmetric multicomponent formulation, Contrib. Mineral. Petrol., 145, 492–501, https://doi.org/10.1007/s00410-003-0464-z, 2003.

Holland, T. J. B. and Powell, R.: An improved and extended internally consistent thermodynamic dataset for phases of petro-

logical interest, involving a new equation of state for solids, J. Metamorph. Geol., 29, 333–383, https://doi.org/10.1111/j.1525-1314.2010.00923.x, 2011.

Johnson, T. and Brown, M.: Quantitative constraints on metamorphism in the Variscides of southern Brittany – a complementary pseudosection approach, J. Petrol., 45, 1237–1259, https://doi.org/10.1093/petrology/egh012, 2004.

Jones, K.-A. and Brown, M.: The metamorphic evolution of the southern Brittany Migmatite Belt, in: Evolution of Metamorphic Belts, edited by: Daly, J.-S., Cliff, R.-A., and Yardley, B.-W.-D., Geological Society Special Publications, vol. 43, 501–505, https://doi.org/10.1144/gsl.sp.1989.043.01.47, 1989.

Jones, K.-A. and Brown, M.: High-temperature "clockwise" P-T paths and melting in the development of regional migmatites: an example from southern Brittany, France, J. Metamorph. Geol., 8, 551–578, https://doi.org/10.1111/j.1525-1314.1990.tb00486.x, 1990.

Lacroix, A.: Matériaux pour la minéralogie de la France. IV. Épidote manganésifère (piémontite) de l'île de Groix, Bull. Soc. fr. Minéralogie, 11, 148–149, 1888.

Lacroix, A.: Contribution à l'étude des gneiss à pyroxène et des roches à wernérite, Bull. Soc. fr. Minéralogie, XII, 83–360, 1889.

Lacroix, A.: Description des gneiss à pyroxène de la Bretagne et des cipolins qui leur sont associés, Bull. Soc. Sci. Nat. Ouest France, I, 173–220, https://gallica.bnf.fr/ark:/12148/bpt6k112500h/f230.item (last access: 12 January 2024), 1891.

Lacroix, A.: Minéralogie de la France et des colonies, Baudry et Cie, Paris, vol. 5, https://gallica.bnf.fr/ark:/12148/bpt6k42205706 (last access: 12 January 2024), 1893–1910.

Lahondère, A., Chèvremont, P., Godard, G., Bouton, P., Béchennec, F., Rebay, G., Santarelli, N., and Viaud, J.-M.: Carte géologique de la France (1/50 000), feuille Palluau (535) + Notice explicative par Lahondère, D., Chèvremont, P., Béchennec, F., Bouton, P., Godard, G., Stussi, J. M., et la collaboration de Viaud, J.-M., Roy, C., Cocherie, A., et Rebay, G., B.R.G.M., Orléans, 171 pp., ISBN 978 2 7159 1535 0, 2009.

Lasnier, B. and Smith, D. C.: A ferro-alumino-taramite- and glaucophane-bearing eclogite from the French Armorican Massif: Ile Dumet, Terra Abstracts, 1, no. 2, 13 Proceedings of the Third International Eclogite Conference, ISSN 0954 4887, 1989.

Le Hébel, F., Gapais, D., Fourcade, S., and Capdevila, R.: Fluid-assisted large strains in a crustal-scale decollement (Hercynian belt of south Brittany, France), in: Deformation Mechanisms, Rheology and Tectonics: Current Status and Future Perspectives, edited by: De Meer, S., Drury, M. R., De Bresser, J. H. P., and Pennock, G. M., Geological Society Special Publications, vol. 200, 85–101, https://doi.org/10.1144/gsl.sp.2001.200.01.06, 2002a.

Le Hébel, F., Vidal, O., Kiénast, J.-R., and Gapais, D.: Les " porphyroïdes " de Bretagne méridionale: une unité de HP-BT dans la chaine hercynienne, C. R. Géosci., 334, 205–211, https://doi.org/10.1016/S1631-0713(02)01746-7, 2002b.

Levillayer, A.: L'île Dumet (Piriac-sur-mer, Loire-atlantique); Histoire et archéologie d'un confetti du Mor Braz, Bulletin et Mémoires Soc. polymathique Morbihan, 146, 27–35, 2020.

Levillayer, A. and Moreau, C.: Un exemple d'archéologie en contexte insulaire ou l'archéologue face à la mer: l'île Dumet (Piriac-sur-Mer, Loire-Atlantique), Mémoires de la Société d'Histoire et d'Archéologie de Bretagne, XCVII, 347–367, ISSN 0750-1420, 2019.

Locock, A. J.: An Excel spreadsheet to classify chemical analyses of amphiboles following the IMA 2012 recommendations, Comput. Geosci., 62, 1–11, 2014.

Lopez-Carmona, A., Abati, J., Pitra, P., and Lee, J. K. W.: Retrogressed lawsonite blueschists from the NW Iberian Massif: P–T–t constraints from thermodynamic modelling and $^{40}Ar/^{39}Ar$ geochronology, Contrib. Mineral. Petrol., 167, 987, https://doi.org/10.1007/s00410-014-0987-5, 2014.

Lotout, C., Pitra, P., Poujol, M., Anczkiewicz, R., and van Den Driessche, J.: Timing and duration of Variscan high-pressure metamorphism in the French Massif Central: A multimethod geochronological study from the Najac Massif, Lithos, 308–309, 381–394, https://doi.org/10.1016/j.lithos.2018.03.022, 2018.

Louail, J.: La Transgression crétacée au Sud du Massif armoricain; Cénomanien de l'Anjou et du Poitou, Crétacé supérieur de Vendée; étude stratigraphique, sédimentologique et minéralogique, Mémoires Soc. Géol. Minéral. Bretagne, 29, 333 pp., 1984.

Marchildon, N. and Brown, M.: Spatial distribution of melt-bearing structures in anatectic rocks from southern Brittany, France: implications for melt-transfer at grain-scale to orogen-scale, Tectonophysics, 364, 215–235, https://doi.org/10.1016/S0040-1951(03)00061-1, 2003.

Martínez Catalán, J. R., Collett, S., Schulmann, K., Aleksandrowski, P., and Mazur, S.: Correlation of allochthonous terranes and major tectonostratigraphic domains between NW Iberia and the Bohemian Massif, European Variscan belt, Int. J. Earth Sci. (Geol. Rundsch.), 109, 269–292, https://doi.org/10.1007/s00531-019-01800-z, 2020.

Paquette, J. L., Ballèvre, M., Peucat, J. J., and Cornen, G.: From opening to subduction of an oceanic domain constrained by LA-ICP-MS U-Pb zircon dating (Variscan belt, Southern Armorican Massif, France), Lithos, 294, 418–437, https://doi.org/10.1016/j.lithos.2017.10.005, 2017.

Palin, R. M., Weller, O. M., Waters, D..J., and Dyck, B.: Quantifying geological uncertainty in metamorphic phase equilibria modelling; a Monte Carlo assessment and implications for tectonic interpretations, Geosci. Front., 7, 591–607, https://doi.org/10.1016/j.gsf.2015.08.005, 2016.

Peucat, J.-J.: Géochronologie des roches métamorphiques (Rb-Sr et U-Pb). Exemples choisis au Groenland, en Laponie, dans le Massif Armoricain et en Grande Kabylie, Mémoires Soc. Géol. Minéral. Bretagne, 28, 158 pp. + 157 pl., 1983.

Pic, A.: Une curiosité géographique: l'île Dumet, in: L'Ile Dumet "Pôle continental" de la terre, edited by: Berget, A., impr. de Commelin fils, Vannes, 7–12, 1936.

Pierronnet, F.-X.: L'île Dumet. Acquisition foncière du Conservatoire de l'espace littoral et des rivages lacustres, Neptunus, 3, 1–7, https://nantes-universite.hal.science/NEPTUNUS/hal-03849742v1 (last access: 12 January 2024), 1997.

Powell, R. and Holland, T. J. B.: An internally consistent thermodynamic dataset with uncertainties and correlations: 3. Applications to geobarometry, worked examples and a computer program, J. Metamorph. Geol., 6, 173–204, https://doi.org/10.1111/j.1525-1314.1988.tb00415.x, 1988.

Quenardel, J.-M., Santallier, D., Burg, J.-P., Bril, H., Cathelineau, M., and Marignac, C.: Le Massif Central/The central massif, Sciences Géologiques, Bulletin, 44, 105–206, 1991.

Richer, É.: Lettre septième: Description du Croisic et d'une partie de la côte voisine, in: Voyage pittoresque dans le département de la Loire-Inférieure, edited by: Richer, É., Mellinet, Nantes, vol. 2, 126 pp., 1820–1823.

Rollando, Y.: Note sur le métamorphisme [du Morbihan], Bull. Soc. polymathique Morbihan, 1951, 32–33, 1951.

Rollando, Y.: Contribution à la minéralogie vannetaise, doctorat, Thèse de pharmacie, Université de Paris, Paris, in-4°, 104 f. dactylographiés + xii pl., 1952.

Smith, D. C.: A review of the peculiar mineralogy of the "Norwegian coesite-eclogite province", with crystal-chemical, petrological, geochemical and geodynamical notes and an extensive bibliography, in: Eclogites and Eclogite-Facies Rocks, edited by: Smith, D. C., Developments in Petrology 12, Elsevier, Amsterdam, 1–206, ISBN 13 978 0444430304, 1988.

Smith, D. C.: Microcoesites and microdiamonds in Norway: an overview, in: Ultra-High Pressure Metamorphism (UHPM), edited by: Coleman, R. G. and Wang, X., Cambridge University Press, Cambridge, 299–355, https://doi.org/10.1017/CBO9780511573088.010, 1995.

Smith, D. C., Godard, G., and Lasnier, B.: Île Dumet (Brittany) and its glaucophane eclogite: the little sister of Île de Groix? Mineralogical Society of Great Britain, Metamorphic Study Group, Meeting "exhumation of metamorphic terranes", Rennes, Abstract volume, p. 77, 1999.

Smye, A. J., Greenwood, L. V., and Holland, T. J. B.: Garnet-chloritoid-kyanite assemblages: eclogite facies indicators of subduction constraints in orogenic belts, J. Metamorph. Geol., 28, 753–768, https://doi.org/10.1111/j.1525-1314.2010.00889.x, 2010.

Triboulet, C.: Coexisting blue and blue-green amphiboles from Ile de Groix (Morbihan, France), J. Petrol., 19, 653–668, https://doi.org/10.1093/petrology/19.4.653, 1978.

Triboulet, C.: Les métabasites entre Concarneau et Lorient: un exemple de métamorphisme prograde polyphasé en Bretagne méridionale, Bull. Minéral., 103, 92–100, 1980.

Triboulet, C.: Uni- and divariant equilibria between staurolite, chloritoid, garnet, chlorite, biotite in medium pressure meta-acidites from Lorient-Concarneau area (South Brittany, France), Contrib. Mineral. Petrol., 82, 195–204, https://doi.org/10.1007/BF01166614, 1983.

Triboulet, C.: Étude géothermo-barométrique comparée des schistes bleus paléozoïques de l'Ouest de la France (Île de Groix, Bretagne méridionale et Bois de Cené, Vendée), C. R. Acad. Sci. Paris (Série 2), 312, 1163–1168, https://gallica.bnf.fr/ark:/12148/bpt6k6293253x/f487.item (last access: 12 January 2024), 1991.

Triboulet, C.: Les schistes verts subglaucophaniques du "Pouldu", zone de transition entre schistes bleus et amphibolites d'un complexe métamorphique monozonal paléozoïque en Bretagne méridionale, C. R. Acad. Sci. Paris (Série 2), 315, 697–703, https://gallica.bnf.fr/ark:/12148/bpt6k6304735s/f711.item (last access: 12 January 2024), 1992.

Triboulet, C. and Audren, C.: Continuous reactions between biotite, garnet, staurolite, kyanite-sillimanite-andalusite and P-T-time-deformation path in micaschists from the estuary of the river Vilaine, south Brittany, France, J. Metamorph. Geol., 3, 91–105, https://doi.org/10.1111/j.1525-1314.1985.tb00307.x, 1985a.

Triboulet, C. and Audren, C.: Évolution des amphiboles et de leurs associations au cours d'un métamorphisme progressif polyphasé dans les métabasites de la Vilaine (Bretagne méridionale), Schweiz. Miner. Petrogr., 65, 279–298, https://doi.org/10.5169/seals-50225, 1985b.

Triboulet, C. and Audren, C.: Les métabasites de l'estuaire de la Vilaine (Bretagne méridionale, France); une série volcano-détritique issue d'une marge continentale active au Paléozoïque inférieur, Hercynica, 1, 55–63, 1985c.

Triboulet, C. and Audren, C.: Controls on $P-T-t$ deformation path from amphibole zonation during progressive metamorphism of basic rocks (estuary of the River Vilaine, South Brittany, France), J. Metamorph. Geol., 6, 117–133, https://doi.org/10.1111/j.1525-1314.1988.tb00412.x, 1988.

Tumiati, S., Martin, S., and Godard, G.: Hydrothermal origin of manganese in the high-pressure ophiolite metasediments of Praborna ore deposit (Aosta Valley, Western Alps), Eur. J. Mineral., 22, 577–594, https://doi.org/10.1127/0935-1221/2010/0022-2035, 2010.

Turrillot, P., Augier, R., and Faure, M.: The top-to-the-Southeast Sarzeau Shear Zone and its place in the late orogenic extensional tectonics of Southern Armorica, Bull. Soc. Géol. France, 180, 247–261, https://doi.org/10.2113/gssgfbull.180.3.247, 2009.

Turrillot, P., Augier, R., Monié, P., and Faure, M.: Late orogenic exhumation of the Variscan high-grade units (South Armorican Domain, western France), combined structural and $^{40}Ar/^{39}Ar$ constraints, Tectonics, 30, TC500, https://doi.org/10.1029/2010TC002788, 2011.

White, R. W., Powell, R., Holland, T. J. B., Johnson, T. E., and Green, E. C. R.: New mineral activity-composition relations for thermodynamic calculations in metapelitic systems, J. Metamorph. Geol., 32, 261–286, https://doi.org/10.1111/jmg.12071, 2014.

Whitney, D. L. and Evans, B. W.: Abbreviations for names of rock-forming minerals, Am. Mineral., 95, 185–187, https://doi.org/10.2138/am.2010.3371, 2010.